# CHARACTERIZATION OF *HELICOBACTER PYLORI* AUTOINDUCER-2 BINDING PROTEINS INVOLVED IN CHEMOREPULSION AND BIOFILM DISPERSAL

by

JENEVA KORYN ANDERSON

A DISSERTATION

Presented to the Department of Chemistry and Biochemistry
and the Graduate School of the University of Oregon
in partial fulfillment of the requirements
for the degree of
Doctor of Philosophy

March 2015

DISSERTATION APPROVAL PAGE

Student: Jeneva Koryn Anderson

Title: Characterization of *Helicobacter pylori* AutoInducer-2 Binding Proteins Involved in Chemorepulsion and Biofilm Dispersal

This dissertation has been accepted and approved in partial fulfillment of the requirements for the Doctor of Philosophy degree in the Department of Chemistry and Biochemistry by:

| | |
|---|---|
| Kenneth Prehoda | Chairperson |
| Karen Guillemin | Advisor |
| Tom Stevens | Core Member |
| Stephen Remington | Core Member |
| Raghuveer Parthasarathy | Institutional Representative |

and

| | |
|---|---|
| J. Andrew Berglund | Dean of the Graduate School |

Original approval signatures are on file with the University of Oregon Graduate School.

Degree awarded March 2015

DISSERTATION ABSTRACT

Jeneva Koryn Anderson

Doctor of Philosophy

Department of Chemistry and Biochemistry

March 2015

Title: Characterization of *Helicobacter pylori* AutoInducer-2 Binding Proteins Involved in Chemorepulsion and Biofilm Dispersal

*Helicobacter pylori* is a human pathogen that colonizes the stomach and increases the risk of diseases such as ulcers and gastric cancer. The distribution of *H. pylori* within the stomach is associated with different disease outcomes, with more dispersed colonization correlated with gastric cancer. The focus of this research is to study the chemotactic responses that promote dispersal of *H. pylori* within the stomach. We have shown previously that *H. pylori* perceive the quorum signal autoinducer-2 (AI-2) as a chemorepellent. We report that *H. pylori* chemorepulsion from endogenous AI-2 influences the proportion and spatial organization of cells within biofilms. Strains that fail to produce AI-2 (Δ*luxS*) or are defective for chemotaxis (Δ*cheA*) formed more spatially homogenous biofilms with a greater proportion of adherent versus planktonic cells than wildtype biofilms. Reciprocally, a strain that overproduced AI-2 ($luxS^{OP}$) formed biofilms with proportionally fewer adherent cells. Along with the known AI-2 chemoreceptor, TlpB, we identified and characterized two novel periplasmic binding proteins, AibA and AibB, that independently both bind AI-2 and are required for the AI-2 chemorepulsion response. Disruptions in any of the proteins required for AI-2 chemotaxis recapitulated the biofilm adherence and spatial organization phenotype of the Δ*luxS* mutant. Furthermore, exogenously administered AI-2 was sufficient to decrease the proportion of adherent cells

in biofilms and promote dispersal of cells from biofilms in a chemotaxis dependent manner. Finally, we found that disruption of AI-2 production or AI-2 chemotaxis resulted in increased clustering of cells in microcolonies on cultured epithelial cells. We conclude that chemotaxis from AI-2 is a determinant of *H. pylori* biofilm spatial organization and dispersal and may play an important role in *H. pylori* colonization of the stomach by promoting dispersal away from areas of high cell density, thereby modulating the disease spectrum of the host.

This dissertation contains previously unpublished, co-authored material.

CURRICULUM VITAE

NAME OF AUTHOR: Jeneva Koryn Anderson

GRADUATE AND UNDERGRADUATE SCHOOLS ATTENDED:

University of Oregon, Eugene, Oregon
Linfield College, McMinnville, Oregon

DEGREES AWARDED:

Doctor of Philosophy, Chemistry, 2015, University of Oregon
Bachelor of Science, Biochemistry, 2009, Linfield College

AREAS OF SPECIAL INTEREST:

Microbiology

GRANTS, AWARDS, AND HONORS:

Science Literacy Program Teaching Fellowship, University of Oregon, 2015

Travel Award, Summer Institute in Statistics and Modeling in Infections Diseases, University of Washington, 2014

Travel Award, Wind River Conference on Prokaryotic Biology, 2013

NIH Molecular Biology Training Grant, University of Oregon, 2010-2013

PUBLICATIONS:

**Jeneva K. Anderson**, Julie Y. Huang, Christopher Wreden, Emily Goers Sweeney, John Goers, S. James Remington, Karen Guillemin. 2015. Chemorepulsion from the Quorum Signal AutoInducer-2 Promotes Helicobacter pylori Biofilm Dispersal. *In review*, mBio.

Emily Goers Sweeney, Nathan Henderson, John Goers, Christopher Wreden, Kevin G. Hicks, **Jeneva K. Foster**, Raghuveer Parthasarathy, S. James Remington, Karen Guillemin. 2012. Structure and Proposed Mechanism for the pH-sensing Helicobacter pylori Chemoreceptor TlpB. Cell Struct. 20:1177-1188

ACKNOWLEDGMENTS

I wish to express sincere appreciation to Professor Karen Guillemin for her continual support for my research, dissertation, and my professional development. In addition, this work was made possible through many meaningful discussions and contributions from Professor Jim Remington, Drs. Emily Goers Sweeney and Christopher Wreden, and Karen Kallio. I'd like to thank the rest of my committee members Professors Kenneth Prehoda, Tom Stevens, and Raghu Parthasarathy for their support throughout my graduate career. Finally, I would like to thank the members of the Guillemin Lab for many fruitful discussions. This work was supported by the National Institutes of Health under award numbers T32GM007759; P50GM098911; and R01DK101314.

For my father: “You've gotten this far, the rest is much easier. The further you go, the easier it gets. You have it, now you've got to believe it. I believe in you.” J.F.

For my husband, Douglas: my continual inspiration in life, love, and science, and the best part of graduate school.

TABLE OF CONTENTS

LIST OF FIGURES

# CHAPTER I

# INTRODUCTION

*Helicobacter pylori* is a Gram-negative bacterium that resides in the human stomach. The prevalence of *H. pylori* infection is approximately 50% worldwide, with higher infection incidences in developing countries (1). Chronic infection with *H. pylori* is linked to various gastroduodenal diseases, including chronic inflammation, peptic ulcers, and in the most severe cases gastric adenocarcinoma and mucosa-associated lymphoid tissue lymphoma (2, 3). The majority of patients infected with *H. pylori* remain largely asymptomatic, but in approximately 10-15% of cases, patients develop peptic ulcers, and in approximately 1% of cases will develop gastric cancer (4). However as of 2012, stomach cancer still remains as the third leading cause of cancer related deaths in both sexes worldwide (5, 6). Thus, much research has been focused on studying *H. pylori* biology and determining effective treatment strategies. The current therapeutic strategy is to treat the infection with a proton pump inhibitor and antibiotics such as clarithromycin, amoxicillin and/or metronidazole (7). However, worldwide increasing levels of antibiotic-resistant *H. pylori* are contributing to failure in treatment of *H. pylori* infection (7). Current research is focusing on alternative strategies to target *H. pylori* to treat the infection before the development of disease in patients.

## *Mechanisms of H. pylori in Promoting Gastric Disease*

*H. pylori* has several known virulence factors that affect host pathways and promote disease states. The most well studied toxins are the virulence proteins CagA and VacA (3). The Cytotoxin-Associated Gene A (CagA) is found in ~70% of *H. pylori*

strains worldwide (3). The *cagA* gene encodes for the CagA protein that is injected by the type-IV secretion system directly into host epithelial cells (8). Once inside the host cells, CagA is able to interact with several host processes, including promoting cell proliferation, differentiation, induction of inflammatory responses, and influence on cell polarity and tight junctions (3, 8). Thus, it is thought that CagA is able to induce abnormalities and overproliferation of cells in the gastric epithelium that are consistent with cancer. The *cagA* gene is highly prevalent in strains of *H. pylori* isolated from patients who are symptomatic for gastric disease; patients with gastric cancer are twice as likely to be infected with a strain of *H. pylori* that carries the *cagA* gene than a *cagA* negative strain (9, 10). Thus, the ability of *H. pylori* to inject this virulence protein into host epithelial cells plays an important role in development of disease in the patient.

The Vacuolating Cytotoxin A (VacA) protein is also highly correlated in strains of *H. pylori* causing disease in patients (11, 12). Receptors on a variety of host epithelial cells are able to bind to VacA, which can influence several cellular processes including pro-inflammatory signaling (11). VacA has also been shown to act intracellularly in host epithelial cells to promote apoptosis, induce vacuole formation inside host cells, alter immune responses, and disrupt cellular pathways including transcriptional regulation (3). Many of these pathways are contributing factors for development of gastric disease. Among the many commonalities between CagA and VacA, one of the most important is that the proteins need to get inside host cells in order to influence the host pathways that contribute to disease. To do so, *H. pylori* needs to be able to establish and persist in the highly acidic organ of the stomach to expose the host epithelial cells to these disease associated proteins.

*H. pylori Persistence in the Human Stomach*

The chemical environment of *H. pylori's* preferable niche is one that many other bacteria cannot tolerate. The stomach is the least colonized region of the gastrointestinal tract, being colonized with $10^1$-$10^3$ CFU/g bacteria (13). It is thought that the high acidity of the organ prevents persistent colonization of most types of bacteria. Within the stomach, there is a gradient of acid that is generated with the highest acidity (pH < 2) in the lumen of the organ, and the least acidity (pH ~ 7) near the epithelial cells (14). A unique feature of *H. pylori* is the production of urease by the cell that is able to neutralize its immediate environment. This allows survival of the cell in the acidic lumen and gives the opportunity for the cell to navigate to its preferred niche of the more neutral pH of the stomach epithelial lining (15), which is perhaps what gives this bacteria an advantage in this sparsely colonized environment.

The strategy of *H. pylori* to navigate to the neutral epithelial cells relies on the ability of the bacterial cell to direct its movement down the proton gradient. To do this, *H. pylori* use a system called chemotaxis to detect and respond to chemicals in the environment. Chemotaxis is a signaling process employed by bacteria to respond to changes in the chemical environment by altering swimming behaviors to swim towards attractive chemicals (chemoattractants) and away from repulsive chemicals (chemorepellents). This signaling system is characterized by a set of proteins that relay extracellular signals (chemoeffectors) to changes in the bacterial flageller motor that alter the rotation of the flagella and modulate swimming behaviors. Chemoeffectors bind to receptors (typically Methylaccepting-Chemotaxis Proteins, MCPs) that are transmembrane receptors. A conserved set of Che proteins reside intracellularly that are

responsible for relaying chemoeffector-receptor binding events to the flagellar motor. The protein CheW binds to the MCP receptor, which in turn allows binding of the histidine kinase CheA. Upon receiving a signal, CheA phosphorylates a cytoplasmic protein CheY; once phosphorylated, CheY can interact with proteins at the flagellar motor to switch the rotation of the flagella and alter the cell's swimming behaviors. CheY quickly becomes dephosphorylated by a protein called CheZ, and loses the interaction with the flagaller motor until it is phosphorylated again by CheA upon a subsequent signaling event. (16) This phosphoregulation pathway allows the bacterial cell to be sensitive to changes in the extracellular chemical environment, and respond rapidly if conditions become unfavorable. *H. pylori* use this system to sense and respond to acid as a chemorepellant; thus, at high proton concentrations, *H. pylori* will orient its movement down the proton gradient until it moves into a more neutral location.

Once at the neutral pH of the stomach epithelium, *H. pylori* colonize in the gastric glands in the antrum of the stomach (17). Normally, *H.* pylori will colonize within the gastric glands in dense communities described as microcolonies (18). This process has been demonstrated in murine models to be dependent on the ability of the *H.* pylori cells to chemotax; chemotactic null mutants are not found in the gastric glands, but instead colonize on top of the epithelial cell layer (19). Thus, chemotaxis plays an important role in guiding *H.* pylori to the neutral stomach epithelium, but also in the way *H. pylori* organize themselves within the stomach epithelium. These differences in spatial localization of *H. pylori* within the stomach are correlated with different disease outcomes in human patients with *H. pylori* infection. A more localized infection of *H. pylori* in the antrum of the stomach is correlated with peptic ulcer diseases, whereas a

more broadly distributed infection of *H. pylori* throughout other areas of the stomach is correlated with more severe gastric cancer disease (4). Thus, this motivates research into understanding the mechanisms that drive dispersal of *H. pylori* in its environment.

Bacteria are able to respond chemotactically not only to host derived environmental cues (in the case of *H. pylori*, acid production by the host), but also to bacterially produced chemicals. *H. pylori* is known to respond to a self-produced quorum-sensing molecule called AutoInducer-2 (AI-2) (20). AI-2 is a small molecule produced by the enzyme LuxS as a by-product of the S-adenosyl-L-methionine pathway (21). Once produced, this molecule is secreted extracellularly into the environment, and is able to be sensed by bacteria, which can elicit a range of responses including chemotactic behaviors. AI-2 is an inter-species quorum-sensing molecule made and sensed by many different types of bacteria (22) that serves as readout of bacterial cell density. For *H. pylori*, AI-2 is perceived as a chemorepellant and will elicit avoidance-swimming behaviors (20). The consequences of this chemorepellant response in *H. pylori* had not been explored in previous work, and the question remained what the role of AI-2 chemorepulsion is in the spatial organization of *H. pylori* within its environment.

In this dissertation, I will discuss my efforts to elucidate the function and mechanism of AI-2 chemotaxis in *H. pylori*. In the following chapter I will discuss my work using an *in vitro* biofilm assay to demonstrate the necessity of AI-2 chemotaxis in the spatial organization of *H. pylori* in biofilms, and the sufficiency of AI-2 to promote dispersal from biofilms in a chemotaxis dependent manner. From this work, I identified two novel proteins in *H. pylori* that are required for the AI-2 chemotaxis response, and discuss further characterization of these proteins in the following two chapters. Finally, I

will put my work into the larger context of *H. pylori* infection and treatment in the final discussion chapter of this dissertation.

The following chapters II and III contain co-authored, unpublished material by myself and collaborators: Julie Huang (Amieva lab, Stanford University) and Dr. Christopher Wreden (Guillemin lab, University of Oregon) who performed the *H. pylori* microcolony assay and analysis in chapter II, and Dr. S. James Remington (University of Oregon) who performed the I-TASSER modeling of AibA and AibB proteins and proposed critical residues for AI-2 binding in chapter III.

# CHAPTER II

# CHEMOREPULSION FROM THE QUORUM SIGNAL AUTOINDUCER-2 PROMOTES *HELICOBACTER PYLORI* BIOFILM DISPERSAL

This chapter contains co-authored material. Julie Huang (Amieva lab, Stanford University) performed the *H. pylori* microcolony infection assay (Figure 5) only. Dr. Christopher Wreden performed data analysis for lacunarity (Figure 1F, Figure 3H) and microcolony size (Figure 5B) only.

## *Introduction*

In nature, bacteria often reside within multispecies aggregate communities called biofilms that serve to protect the cells from environmental challenges (23–27). Within these aggregated communities, bacterial cells secrete molecules that allow the biofilm to grow at environmental interfaces and attach to other cells and biotic or abiotic surfaces (28, 29). The persistence of biofilms on biotic surfaces, such as the lung epithelia of cystic fibrosis patients, or on abiotic surfaces, such as medical implants, poses serious human health risks (26, 30–32). Despite the medical importance of biofilm growth, many unanswered questions remain about the mechanisms that drive biofilm dynamics.

Biofilm formation is initiated by attachment of single cells to a surface, and these adherent cells grow as clonal populations into microcolonies. These microcolonies can further develop into mature biofilms with distinct cellular organization and structures (26). This process is dynamic, with continuous joining and leaving of cells in response to changes in the environment (28, 31). The biofilm lifecycle involves cellular processes

that occur over different time scales, and require long-term cell fate commitments as well as a need for bacterial cells to respond quickly to changes in the environment.

In many bacterial species, biofilm formation is influenced by quorum sensing, a mechanism bacteria use to coordinate their behavior (22, 33, 34). Quorum sensing involves the production of small molecules that are secreted into the environment and sensed by other bacterial cells in a population density dependent manner (22). Often the recipient bacteria respond to quorum sensing molecules by inducing changes in gene expression, such as those involved in long-term commitment to a sessile or planktonic lifestyle (22). For example, quorum sensing regulated genes are involved in the production of exopolysaccharides, lipids, nucleic acids, and proteases that are required to build the biofilm matrix (35–38).

Quorum sensing can also elicit more immediate changes in bacterial behaviors by directing cellular motility through chemotactic responses. For example, in the predatory bacterial species *Myxococcus xanthus,* a secreted small molecule called A-factor alters motility and promotes aggregation and the initiation of fruiting body biofilm formation (39–41). Importantly for this study, the quorum sensing molecule AutoInducer-2 (AI-2), an interspecies quorum sensing molecule produced by the conserved metabolic enzyme LuxS, elicits chemotactic responses in multiple bacteria (20, 42). In the enteric commensal *Escherichia coli*, AI-2 elicits an attractant response (42), whereas in the gastric pathogen *Helicobacter pylori,* AI-2 is sensed as a repellant (20). In this study, we address how these rapid responses to quorum sensing molecules influence spatial distributions of cells within a biofilm community.

To explore this question, we studied the role of AI-2 chemotactic responses in *H. pylori* biofilm formation on abiotic and biotic surfaces. Previous work has shown that *H. pylori* form microcolonies and biofilms both *in vitro* on cultured epithelial cells as well as *in vivo,* as revealed in human stomach biopsies (18, 19, 43–47). Relevant to our study, Cole *et al.* showed that a *luxS* deficient *H. pylori* mutant exhibited increased levels of adherence to glass frit relative to a wild type strain (44). Here we replicate this finding and test whether it is due to loss of an endogenously produced chemorepulsive cue. We investigate the impacts of AI-2 production and sensing during early and late stages of biofilm growth and show that AI-2 chemotaxis is an important modulator of the equilibrium between planktonic and biofilm cells and the spatial distribution of cells within the biofilm. We define the molecular basis for AI-2 chemoreception in *H. pylori*, identifying two new periplasmic AI-2-binding binding proteins that are essential for this process. Additionally, we demonstrate that disruption of AI-2 production or AI-2 chemotaxis results in increased microcolony size of *H. pylori* on cultured epithelial cells. Our work supports a novel mechanism whereby rapid chemotactic responses of individual cells to quorum sensing molecules contribute to the long-term spatial organization and aggregation properties of biofilms.

## *Results*

### *AI-2 production and chemotaxis influence biofilm organization*

To investigate the importance of AI-2 chemorepulsion for *H. pylori* biology, we examined *H. pylori* biofilm organization as a function of AI-2 production. We spotted liquid cultures of G27 wild type (WT) and isogenic Δ*luxS* strains of *H. pylori* onto sterile

glass slides, which were cultured under static, humidifying microaerobic conditions for five days. The biofilms that formed at the air-liquid interface were fixed, stained with the DNA dye 4',6-diamidino-2-phenylindole (DAPI), and imaged using fluorescence microscopy (Fig. 1A-E). Upon visualization, it was immediately apparent that wild type and Δ*luxS* cells differed in their spatial distributions in biofilms. WT cells formed discrete multicellular aggregates, whereas the Δ*luxS* cells formed a homogeneous mat of cells (Fig. 1A,B). Genetic complementation of *luxS* (*luxS*$^{*}$) was able to restore biofilm organization to the WT pattern (Fig. 1C). This result suggests that LuxS is required for normal multicellular organization within biofilms. We next wanted to test if increasing endogenous AI-2 production would alter the cellular organization in biofilms. We engineered a strain with an extra chromosomal copy of the *luxS* gene (*luxS*$^{OP}$, over-producer) expressed from the native *luxS* promoter and confirmed that this strain grew with similar kinetics to WT (Fig. A1A) and produced more AI-2 (Fig. A1B). Upon biofilm visualization, we observed that the *luxS*$^{OP}$ strain had cellular organization similar to that of WT (Fig. 1D).

Fractal dimension and lacunarity have been used to quantify differences in spatial organization of biofilms (48, 49). Fractal dimension describes the complexity of the image while lacunarity measures the extent of discontinuities or inhomogeneity of the image (48). We used FracLac (an ImageJ plug-in) to calculate fractal dimension and lacunarity score for epifluorescence images of biofilms that were thresholded using contrast-limited adaptive histogram equalization (Fig. A2). Although we observed no difference in fractal dimension between any of the strains (data not shown), we did observe differences in lacunarity scores that correlate with perceived differences in the

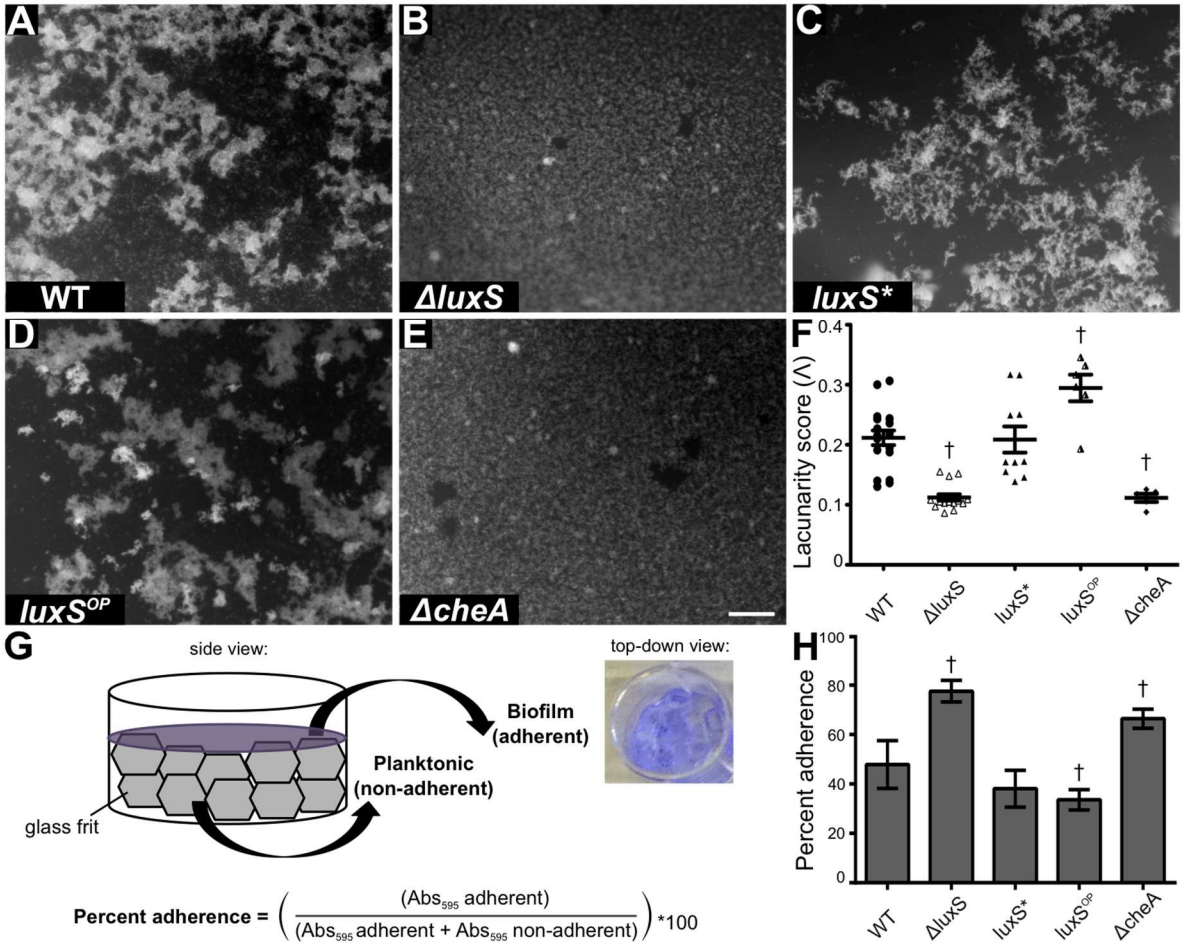


**Figure 1: Endogenous AI-2 production and chemotaxis alter biofilm organization.** (A-E) Epifluorescence images of wild type and mutant G27 *H. pylori* biofilms grown on glass slides for 5 days. Cells were fixed and stained with DAPI (white). Scale bar is 100 μm. (F) Lacunarity scores for biofilm images. Each dot represents the lacunarity score of a single epifluorescence biofilm image post thresholding, with corresponding mean and standard deviation. (G) Schematic of glass frit biofilm assay with crystal violet analysis and example percent adherence calculation. (H) Effect of AI-2 production and chemotaxis on adherence of cells in biofilms on glass frit after five days, as quantified by the crystal violet assay. Error bars represent standard error of the mean for a minimum of three experiments for each strain. Daggers indicate a significant difference ($p < 0.05$) from wild type using a Student's T-test (F) or one-way analysis of variance (H).

images (Fig. 1F). *ΔluxS* had a significantly lower lacunarity score compared to WT, indicating more homogeneity. Reciprocally, the lacunarity score was significantly higher for *luxS*$^{OP}$ than WT, indicating more spatial inhomogeneity. We conclude that the spatial organization of cells in biofilms is dependent on levels of AI-2 production.The overall biofilm structure is the result of dynamic interactions of cells transitioning between sessile and planktonic states. We wished to quantify the fraction of the population in each of these states. To do so, we grew *H. pylori* cultures under static, microaerobic conditions in wells filled with glass frit to provide abundant surfaces for biofilm formation (Fig. 1G). After two days, we used crystal violet staining to determine the proportion of adherent and planktonic cells for both WT and *luxS* derivatives (adapted from (44)) (Fig. 1H). We observed that the Δ*luxS* strain had a significantly higher proportion of adherent cells as compared to WT and the *luxS*$^{*}$ strains. In addition, the *luxS*$^{OP}$ strain produced biofilms with a modest, but significant reduction in the proportion of adherent cells as compared to wild type biofilms. Together, these results suggest that normal biofilm formation and organization of *H. pylori* G27 are modulated by levels of endogenously produced AI-2.

We hypothesized that the differences in biofilm organization we observed were due to chemorepulsion from endogenously produced AI-2. To test this, we investigated biofilm formation of a chemotaxis deficient strain, Δ*cheA*, which lacks the signal transduction protein CheA required for actuating chemotactic responses. The cellular organization of Δ*cheA* biofilms resembled those observed with the Δ*luxS* strain with uniform films of cells (Fig. 1E) and a significantly lower lacunarity score compared to WT (Fig. 1F). Consistent with this observation, the Δ*cheA* mutant displayed increased

proportional adherence as compared to WT (Fig. 1H). This indicates that chemotaxis plays an important role in dictating cellular organization and adhesion within *H. pylori* biofilms.

*Chemotactic responses to AI-2 require two novel periplasmic AI-2 binding proteins*

Because LuxS functions as both a quorum signal synthase and a metabolic enzyme (50), the biofilm defects of the Δ*luxS* could be due to additional cellular phenotypes other than loss of AI-2 chemorepulsion. To better test our hypothesis that biofilm organization is modulated by AI-2-induced chemorepulsion, we sought to identify the proteins specifically involved in AI-2 chemorepulsion in *H. pylori*. In *E. coli*, AI-2 chemotaxis requires the chemoreceptor Tsr and the periplasmic binding protein LsrB (42). We have previously shown that in *H. pylori*, AI-2 chemorepulsion requires the chemoreceptor TlpB (20), however there is no homolog of LsrB in *H. pylori* as determined by BLAST protein sequence alignment (51). Chemoreceptors signal via direct ligand binding or through interactions with ligand binding proteins that transduces signals to the chemoreceptor (52). Given the lack of a LsrB homolog in *H. pylori*, we assessed whether TlpB could bind AI-2 directly. We adapted an *in vitro* AI-2 binding assay (53, 54) in which AI-2 was incubated with either the purified periplasmic portion of TlpB or purified LsrB protein as a positive control. To quantify AI-2 binding, proteins were purified away from unbound AI-2, denatured to release bound AI-2, and the supernatant was used to stimulate *V. harveyi* luminescence. As expected, the luminescence levels induced by the LsrB supernatant were high, indicating the presence of bound AI-2 (Fig. 2B). By contrast, the luminescence levels stimulated by TlpB were

not above background levels. This suggests that TlpB does not bind AI-2 directly *in vitro* and may require additional proteins.

We hypothesized that a periplasmic binding protein (PBP) in *H. pylori* performs a similar function as LsrB. We identified five hypothetical proteins in G27 that were homologous to other periplasmic transport and binding proteins: HPG27_277, HPG27_431, HPG27_889, HPG27_1116, and HPG27_1197. We tested these potential candidates for their requirement in AI-2 chemorepulsion by making non-polar deletions of each PBP individually via allelic exchange and assessed the ability of these mutants to respond to AI-2. We tested the chemorepellant responses of these mutants to 100 μM AI-2 using a previously described barrier assay (20). In this assay, formation of a barrier of swimming cells away from the source of the chemical indicates a repellent response. We discovered that two of the five PBP mutants, ΔHPG27_277 and ΔHPG27_431, could form barriers to another known chemorepellant, HCl, but formed no barrier in response to AI-2 (Fig. 2A). These results suggest that both of these putative PBPs are independently required for AI-2 chemotaxis. The other three PBP mutants remained responsive to AI-2 (data not shown).

Using the *in vitro* AI-2 binding assay described above, we tested the ability of these two proteins to bind AI-2. For this assay we constructed HPG27_277 and HPG27_431 variants lacking their hydrophobic periplasmic targeting sequences for ease of purification. We observed significant AI-2 binding capacity for both HPG27_277 and HPG27_431 proteins, similar to the LsrB positive control (Fig. 2B). These results indicate that both HPG27_277 and HPG27_431 bind AI-2 directly *in vitro* and independently of one another. Due to this identified function, HPG27_277 and

HPG27_431 will be called AibA and AibB, respectively, for **AI**-2 **B**inding proteins A and B.

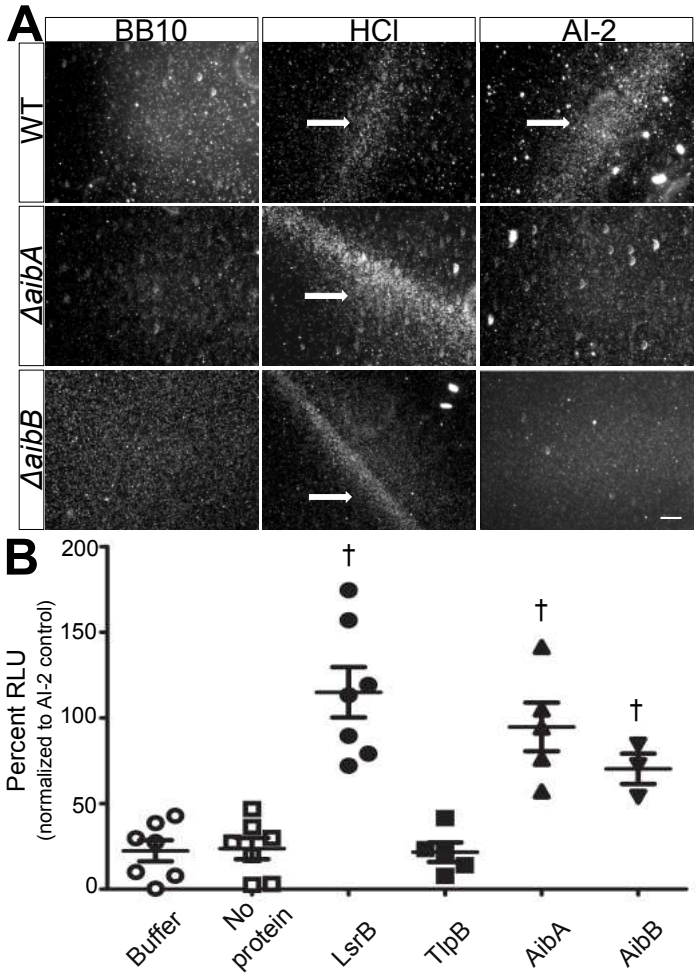


**Figure 2: AI-2 chemotaxis requires two periplasmic binding proteins, AibA and AibB, that bind AI-2 independently.** (A) Chemotaxis response of wild type, Δ*HPG27_277* (Δ*aibA*) and Δ*HPG27_431* (Δ*aibB*) mutant *H. pylori* to Brucella broth (BB10), 100 mM HCl and 100 μM synthetic DPD (AI-2). Shown are representative wet mount images of bacterial cells (white dots). Formation of a barrier (indicated in white arrows) indicates a chemorepellant response. Scale bar is 200 μm. (B) *In vitro* AI-2 binding assay with purified proteins using a *V. harveyi* bioluminescence readout. Percent relative luminescence units are normalized to an AI-2 positive control in each independent experiment. Error bars represent the standard error of the mean between experiments. Daggers indicate a significant difference ($p < 0.05$) from the no buffer negative control using a Student's T-test.

*TlpB, AibA and AibB are necessary for biofilm organization*

To further test the hypothesis that AI-2 chemotaxis influences spatial organization of cells within biofilms, we observed biofilms of strains lacking AI-2 chemoreception (Δ*tlpB,* or the PBPs Δ*aibA* or Δ*aibB*, or the double Δ*aibA*;Δ*aibB* mutant) grown on glass slides, as previously described (Fig. 3A-G). We found that the cellular organization of all three AI-2 chemotaxis deficient strains (Fig. 3A,C,E,G) recapitulated the biofilm structures of the Δ*luxS* and the Δ*cheA* deficient *H. pylori* strains. Consistent with this observation, the lacunarity scores for the biofilms of these strains were significantly lower than WT (Fig. 3H), and similar to scores observed with Δ*luxS* and Δ*cheA* strains (compare to Fig. 1F). We also quantified the proportion of adherent and planktonic cells within 48-hour biofilms of Δ*tlpB,* Δ*aibA*, Δ*aibB,* and Δ*aibA*;Δ*aibB* strains grown on glass frit and found that the AI-2 chemotaxis deficient strains had significantly increased proportional adherence in biofilms compared to WT (Fig. 3I) and similar to the Δ*luxS* and Δ*cheA* strains (compare to Fig. 1H).

We next attempted to complement these biofilm defects in the AI-2 chemotaxis deficient strains. Genetic complementation in *H. pylori* is limited by the precision with which genes can be expressed from heterologous loci. To complement TlpB, we made use of an engineered mutation ($TlpB^{D114N}$, (55)) in the endogenous locus that we have shown disrupts acid sensing but not AI-2 chemorepulsion. We found that this variant of TlpB was able to restore normal proportion of adhesion in the biofilm (Fig. 3I), but it did not rescue the cellular organization phenotype (Fig. 3B) or the lacunarity of the biofilms (Fig. 3H). Complementation of *aibA* deficiency was achieved by inserting the wild type

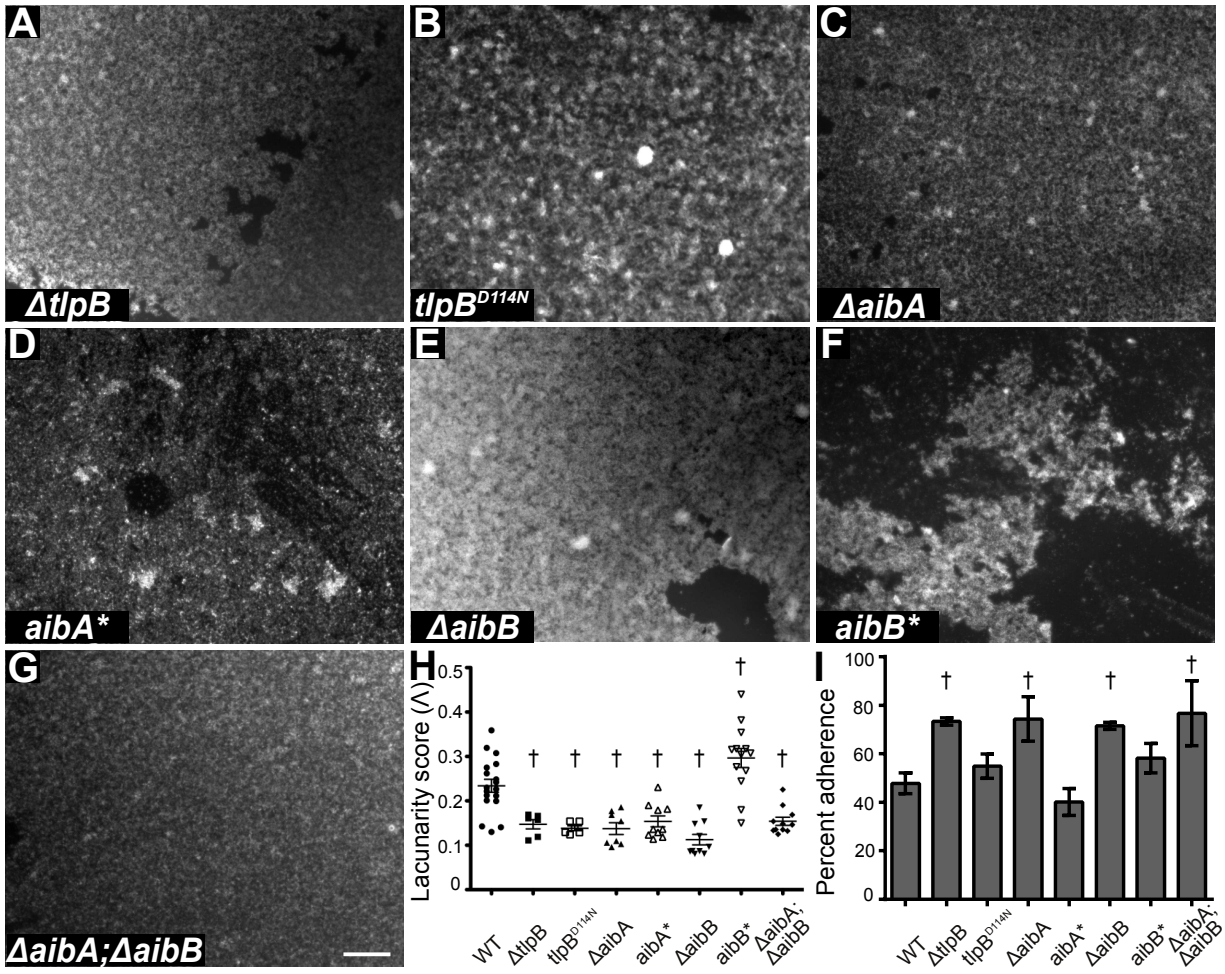


**Figure 3: Chemorepulsion from AI-2 is necessary for biofilm organization.** (A-G) Epifluorescence images of AI-2 chemotaxis defective mutants and complemented strain biofilms grown on glass slides for 5 days. Cells were fixed and stained with DAPI (white). (H) Lacunarity scores for biofilm images. Each point represents the lacunarity score of a single epifluorescence biofilm image post thresholding, with corresponding mean and standard deviation. (I) Effect of AI-2 chemotaxis disruption on adherence of cells in biofilms on glass frit after five days, as quantified by the crystal violet assay. Error bars represent the standard error of the mean for a minimum of three experiments for each strain. Daggers indicate a significant difference ($p<0.05$) from wild type using a Student's T-test (H) or a one-way analysis of variance (I).

*aibA* gene at the *rdx* locus (*aibA**). Due to *aibA* being part of a potential operon, we engineered the putative *aibB* promoter into the *rdx* locus to drive expression of *aibA*. As with TlpB, complementation of *aibA* did restore proportional adhesion in the biofilm (Fig. 3I), but was unable to rescue the Δ*aibA* mutant spatial organization (Fig. 3D,H).

Complementation of Δ*aibB* was also achieved by restoration of the wild type gene and putative promoter at the *rdx* locus (*aibB**). In this case, complementation restored the normal proportional adhesion (Fig. 3I) and was able to rescue the spatial organization of cells in the biofilm back to the WT spatial patterning (Fig. 3F), with a slightly higher lacunarity score than WT (Fig. 3H; p=0.04 by Student's T-test).

We hypothesized that the partial rescue in lacunarity observed in the *aibA** and $tlpB^{D114N}$ strains may be due to decreased transcript or protein levels compared to WT. To address this, we used qRT-PCR to quantify the relative amount of *aibA, aibB and tlpB* transcripts in the complemented strains compared to WT (Fig. A3; see the appendix for all figures with an "A" designation). We observed that the levels of *aibB* in the *aibB** strain was roughly WT levels (Fig. A3, $WT_{aibB}$ and *aibB**), and indeed we observe full rescue of biofilm phenotypes with this strain (Fig. 3F,H,I). The levels of *aibA* in the *aibA** strain were approximately 60% of levels of *aibA* in WT (Fig. A3, $WT_{aibA}$ and *aibA**). This may explain why we observed incomplete rescue of the spatial organization and lacunarity of *aibA** biofilms (Fig. 3D,H). We observed that the $tlpB^{D114N}$ complement has similar levels of *tlpB* transcript as in WT (Fig. A3, $WT_{tlpB}$ and $tlpB^{D114N}$), consistent with WT levels of protein expression in this strain (55). However, this study also showed that the $TlpB^{D114N}$ protein is less stable than the WT TlpB protein *in vitro*, which could explain the incomplete rescue of the $tlpB^{D114N}$ biofilm spatial organization and lacunarity (Fig. 3B,H).

*AI-2 is sufficient to alter biofilm organization during biofilm formation in a chemotaxis dependent manner*

Having demonstrated that AI-2 production and chemotaxis are necessary for normal biofilm formation, we next wanted to extend our findings by manipulating the system with exogenously added AI-2. To accomplish this, we added AI-2 at the time of inoculation of cells into wells containing glass frit and quantified the difference in percent adherence (Fig. 4A). We determined empirically that 37nM AI-2, a concentration within the range produced by *H. pylori* endogenously (56), caused the greatest effect in these assays, and we used this concentration in all subsequent experiments. We found that exogenous AI-2 reduced the proportion of adhered WT *H. pylori* when measured 48 hours after initiation of biofilm formation and AI-2 addition. We also observed a significant reduction in adherence for the Δ*luxS* strain upon addition of AI-2. This is consistent with the fact that although the *luxS* deficient strain is unable to produce AI-2, it can still respond to exogenous AI-2 (56). Next we performed this experiment with the AI-2 chemotaxis deficient strains Δ*cheA,* Δ*tlpB*, Δ*aibA*, and Δ*aibB*. Consistent with the inability of these strains to sense AI-2, they exhibited no differences in the proportion of adherent cells in the presence or absence of exogenous AI-2. These results indicate that biofilm organizational patterning induced by AI-2 requires intact AI-2 sensing and that AI-2 is sufficient to decrease adherence in biofilms during the early stages of biofilm formation.

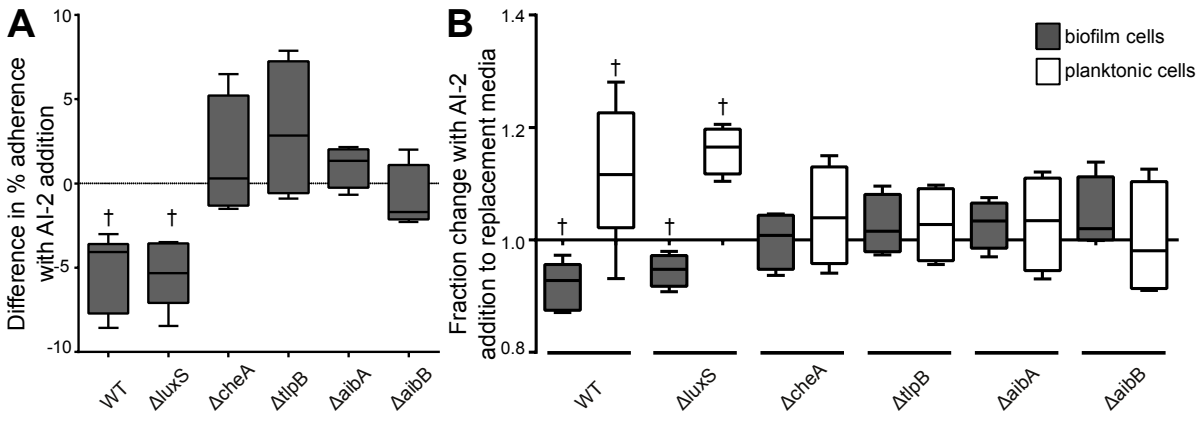


**Figure 4: Chemorepulsion from AI-2 is sufficient to decrease adherence in biofilms.** (A) Change in adherence of strains in biofilm with addition of exogenous AI-2 (37 nM) at time of inoculation. Daggers indicate a significant difference ($p<0.05$) from 0 (no change) using Student's T-test. (B) Fraction change in biofilm size (grey bars) and number of planktonic cells (white bars) measured 72 hours after the initiation of the biofilms and 24 hours after replacement of media containing 37 nM exogenous AI-2. Daggers indicate significant difference ($p<0.05$) from 1 (no change) using a Student's T-test. Box plots show the mean and standard deviation for a minimum of three experiments for each strain.

We next tested directly whether AI-2 chemotaxis acted to decrease adherence in biofilms by promoting dispersal from mature biofilms. We grew biofilms of WT and Δ*luxS* for 48 hours, gently removed the media containing planktonic cells, and replaced it with fresh media either with or without exogenous AI-2 (37 nM). At this time point, adherent cells were readily visible on the sides of the well and on the glass frit. After another 24-hour incubation, we quantified the populations of planktonic and adherent cells. Because we removed planktonic cells from the wells at 48 hours, we assumed that all cells entering the planktonic population after media replacement were ones that dispersed from the pre-existing biofilm. We calculated the change in the biofilm (adherent) population between cultures treated with AI-2 versus untreated controls and separately calculated the change in the planktonic (non-adherent) population between the two treatment groups (Fig. 4B). Both WT and Δ*luxS* strains exhibited a decrease in their

biofilm populations upon AI-2 addition, suggesting that AI-2 was sufficient to have triggered partial biofilm dispersal. Reciprocally, there was an increase in the number of the planktonic cells of these two strains upon addition of AI-2. To confirm the role of chemotaxis in AI-2-mediated biofilm dispersal, we examined the response of the Δ*cheA,* Δ*tlpB,* Δ*aibA,* and Δ*aibB* mutant biofilms to AI-2 addition. We found no significant difference in the biofilm or the planktonic populations of any of these strains upon the addition of AI-2. These results indicate that AI-2 promotes dispersal of cells from pre-existing biofilms by a chemotaxis dependent mechanism.

*Abolishing AI-2 production or AI-2 chemotaxis results in larger microcolony formation on cultured epithelial cells*

We wanted to test whether this AI-2 chemotaxis response was relevant to the fitness of *H. pylori* on epithelial cells where they will experience a different set of chemical signals than on abiotic surfaces. To do this, we adapted a previously described microcolony assay (18) using polarized Madin-Darby Canine Kidney (MDCK) epithelial cells seeded onto a transwell filter. We used the G27MA strain, which had been adapted to grow well on MDCK cells (57), in contrast to the parental G27 strain that does not grow well in this assay (data not shown). We infected MDCK monolayers with WT G27MA and isogenic Δ*luxS*, Δ*cheW* (a functionally similar mutant to Δ*cheA*), Δ*tlpB,* Δ*cheA,* Δ*aibA,* and Δ*aibB* strains to test if AI-2 production or chemotaxis influenced the size of microcolonies formed. The attached bacteria grow on the epithelial cells and form aggregates or microcolonies. We hypothesized that similar to what we observed in the *in*

*vitro* biofilm formation, that we would expect increased dispersal of cells from microcolonies in an AI-2 chemotaxis dependent manner.

To do this, we fixed and stained the transwells to visualize *H. pylori* cells and MDCK cell junctions at 5 minutes post infection (initial attachment) and at 3 days post infection (Fig. 5A-C). To determine if all strains had equivalent growth and attachment on the MDCK cells, we estimated the attached bacteria on the cell layer at 5 minutes and 3 days post infection. To do this, we quantified the average microcolony sizes of cells in at least 3 fields of triplicate transwells for each condition and used the size measurement of a single *H. pylori* cell (20 pixels) to estimate the number of *H. pylori* cells in the image. We then extrapolated this to estimate the number of attached *H. pylori* cells in the entire transwell (Fig. 5D). We observed that the WT, Δ*luxS*, and Δ*tlpB* strains had significantly increased numbers of attached bacteria from 5 minutes to 3 days post infection. However, for Δ*cheW*, Δ*cheA*, Δ*aibA*, and Δ*aibB* strains, we observed no significant increase in attached bacteria over the course of the experiment. There are several possible explanations for this observation, including lack of growth on the MDCK cells, defects in attachment, or increased dispersal of cells from microcolonies. Given the ambiguity of these strains in this assay, we were unable to interpret and evaluate these strains using this assay.

For the WT, Δ*luxS* and Δ*tlpB* strains that were able to grow equivalently in this assay, we measured the average microcolony size from 5 minutes to 3 days post infection (Fig. 5E). We found that the Δ*luxS* strain had a significant increase in microcolony size at 3 days post infection compared to WT, while there was no significant difference in initial attachment (Fig. 5E). Thus, disruption *of luxS* results in increased aggregation, which is

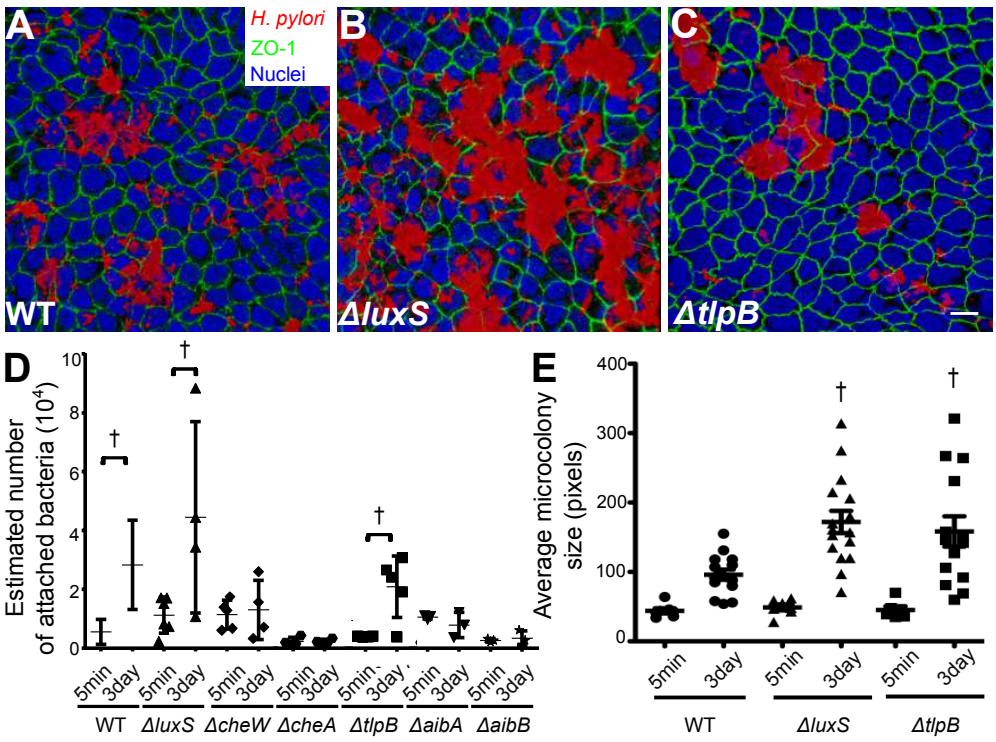


**Figure 5: Disruption of either AI-2 production or AI-2 chemotaxis results in larger microcolonies on cultured epithelial cell monolayers.** (A-C) Representative images of WT, Δ*luxS*, Δ*cheW*, and *ΔtlpB H. pylori* microcolonies on polarized MDCK monolayers at 3 days post-infection. *H. pylori* cells are visualized in red, nuclei in blue, and cell junctions in green. Scale bar is 10μm. (D) Estimated number of attached bacteria on MDCK epithelial cell layer at 5 minutes and 3 days post infection for all strains. Each point represents the estimated number of bacteria averaged over multiple images per transwell. Error bars represent the standard error of the mean. Daggers represent statistical significant increase in number of attached bacteria from 5 minute to 3 day attachment for each strain. (E) Plot of microcolony area, in units of pixels, for each strain at 5 minutes and 3 days post inoculation. Each dot represents the average size of all the colonies in an image, in pixels. Three images were taken per transwell, with three replicate transwells per experiment. Error bars represent standard error of the mean. Daggers represent statistical significance of pixel sizes ($p<0.05$) from WT through a one-way analysis of variance.

consistent with our observations in the *in vitro* biofilm assays (Fig. 1H). Also consistent with our predictions, we observed that the lack of *tlpB* resulted in microcolony sizes significantly larger than WT and similar to the Δ*luxS* strain (Fig. 5E). Taken together,

these results suggest that AI-2 chemorepulsion is important for promoting *H. pylori* dispersal from cell aggregates on epithelial cell surfaces.

## *Discussion*

For many bacterial species, quorum sensing has been well characterized to influence biofilm formation through the regulation of gene expression. Here we introduce a new role for quorum sensing in shaping biofilms on a much more rapid time scale through chemotactic responses of cells to quorum signals. We provide evidence that *H. pylori* biofilm dispersal and cellular spatial organization is shaped by chemorepulsive responses to AI-2 in *H. pylori*.

### *H. pylori uses a novel AI-2 sensing mechanism*

Although many bacterial species produce and sense AI-2, mechanisms for AI-2 sensing are not strictly conserved among them. Prior to this work, two examples had been described for AI-2 sensing: one through the periplasmic LuxP binding partner of the LuxQ histidine kinase in *Vibrio* species, and a second through the PBP LsrB in several phylogenetically distinct families, which serves as both an AI-2 transport protein and binding partner for the chemoreceptor Tsr (53, 58, 59). In this study, we investigated the molecular basis for AI-2 chemoreception in *H. pylori* and discovered two PBPs, AibA and AibB, that are both independently required for AI-2 perception. AibA and AibB are conserved at greater than 95% identity at the amino acid sequence level throughout *H. pylori* species. Protein sequence homology identifies AibA as homologous to dipeptide binding proteins (39% identity with *E. coli* dipeptide binding protein, Protein Data Bank ID 1DPP) and AibB as homologous to molybdate binding proteins (36% identity to

*Azotobacter vinelandii* periplasmic molybdate-binding protein, Protein Data Bank ID 1ATG). However, to our knowledge this study is the first to demonstrate a function of these proteins. Despite the shared function of AI-2 binding, AibA, AibB, LsrB and LuxP show little conservation in amino acid sequence (Fig. A4). We predict that other bacteria may also have chemotactic responses to AI-2 that have not yet been identified due to the lack of sequence homology among AI-2 binding proteins.

The requirement of two PBPs for AI-2 perception is novel for chemotransduction and uncommon in signal transduction in general. In *Pseudomonas aeruginosa*, the FpvCDEF system for iron uptake requires two PBPs, FpvC and FpvF. However, in this system, a FpvC/FpvF complex is required for binding to ferric compounds (60). In contrast, AibA and AibB both bind AI-2 independently *in vitro* (Fig. 2B). We do not yet know if AibA and AibB form a complex in the cell and if so, in what stoichiometries, but this is a possible model for the chemorepellant response in *H. pylori* that we plan to explore in future work.

*Responses to AI-2 on different time scales promote biofilm dispersal*

Cell dispersal from biofilms is an important part of the life cycle of these structures. Although cells in biofilms benefit from protection from environmental stressors, a sedentary lifestyle is not always advantageous. It may be beneficial for cells to leave the biofilm if there are abundant external resources available or if resources are depleted at the biofilm site. The dispersal of cells from biofilms in response to chemical cues can be described as “bet hedging”, which is an evolutionary response to changes in environments (61). When the chemical cue driving dispersal is endogenously produced

and proportional to cell density, this provides a mechanism to maximize the ability of a population to explore new habitats and avoid depleting resources at the original site.

Cells can promote their dispersal from biofilms via several mechanisms that involve processes over different time scales. A common mechanism for dispersal involves the down regulation of matrix producing proteins and the up regulation of enzymes (proteases, DNases, etc.) to degrade extracellular polymeric substances and nucleic acids that form the adherent matrix between cells of the biofilm (62, 63). Several bacterial species upregulate motility-associated genes, such as those required for flagellar biosynthesis, at the onset of dispersal (63). However, these mechanisms require changes in gene expression that take place over a time scale of minutes to hours. A mechanism for more rapid dispersal from biofilms is known as seeding dispersal, which has been shown to contribute to the virulence of several bacterial pathogens. Biofilms of *Pseudomonas aeruginosa*, *Staphylococcus aureus* and others (63) form hollow cavities containing non-adherent, motile cells. Upon weakening of the extracellular matrix, these planktonic cells exit the biofilm in large numbers. Our work showing that chemotactic responses, which occur on the timescale of seconds to minutes, also provides a rapid mechanism for bacteria to exit a biofilm. We speculate that this would allow the structure to be much more plastic and adaptable to rapid fluctuations in the external or internal environment of the biofilm. It is likely that cells use multiple mechanisms of dispersal to orchestrate their exit from the biofilm when it is most advantageous to do so.

*The spatial patterning of chemical cues can influence biofilm formation*

*H. pylori* cells encounter a diversity of host and microbial derived signals in their native environment of the human stomach, the integration of which will determine their spatial distribution. Our experiments demonstrate that AI-2 chemotactic responses are necessary and sufficient for modulating *H. pylori* biofilm formation. We observed similar requirements for AI-2 production and reception for biofilms grown on glass frit or for microcolonies grown on epithelial cells. However, we noted that the majority of chemotaxis deficient strains were less able to attach or grow well on the MDCK cells. Previous work has shown that *H. pylori* uses chemotaxis as a guide to interact with the mouse stomach epithelium (64). In our system, we hypothesize that epithelial cells provide *H. pylori* more attractive cues than glass frit, and thus chemoattraction would play a more important role in the seeding of microcolonies on the epithelial surface than in the glass frit biofilm assay. Thus, in the case of growth on epithelial cells, the loss of chemotaxis would eliminate both attractive and repulsive drivers of microcolony formation, whereas on the glass frit only repulsive responses would be lost. This may explain the differences in attachment of the chemotaxis mutants on the abiotic versus biotic surfaces.

Our results also provide insights into the spatial patterning of AI-2 during biofilm formation. We observed that adding exogenous AI-2 to a wild type and Δ*luxS* culture was sufficient to decrease the proportion of adherent cells in biofilms, however this exogenous AI-2 addition to the Δ*luxS* culture could not fully restore proportional adherence back to wild type levels. We assume that the bulk addition of AI-2 at a single time point does not accurately recapitulate the concentrations and spatial distributions of

endogenously produced AI-2 experienced by cells in the growing biofilm. Indeed, we observed stronger effects on biofilm structures by genetically manipulating the cells to overproduce AI-2 than when we added the chemical exogenously. We predict that small or stochastic changes in the AI-2 environment during biofilm growth can alter the overall structure of the biofilm as it grows.

A striking effect of the loss of AI-2 production or sensing is the more homogenous spatial organization of the biofilms grown on glass, which appear to be uniformly dispersed throughout the biofilm, rather than heterogeneous clumps interspersed with sparse areas. We hypothesize that local fluctuations in AI-2 concentrations are important determinants of the spatial heterogeneities that are characteristic of wild type *H. pylori* biofilms. One could even imagine a positive feedback loop in which stochastic fluctuations in AI-2 concentration would give rise to different local dispersal frequencies, creating heterogeneities in cell density that would enhance local variations in AI-2 concentrations. Interestingly, previous studies have shown that *luxS* expression in sessile biofilm populations is high for the first two days, but decreases significantly in the biofilm cells after this time point (65, 66). Such a down-regulation of *luxS* could mark a transition to a more mature biofilm stage with less cell dispersal. The spatial heterogeneities observed in our wild type *H. pylori* biofilms resemble those described in other biofilm systems to be critical for nutrient and waste product flux and the overall fitness of the organisms within the biofilm structure (40). We speculate that because AI-2 chemorepulsion can operate on a rapid timescale and is sensitive to subtle spatial and temporal fluctuation in AI-2 concentration, it serves as an

important mechanism for generating the spatially heterogenous distribution of cells in a mature biofilm.

*Chemotactic responses to quorum sensing molecules as determinants of multi-species biofilm organization*

The dynamics of biofilm formation and maturation require complex, sequential mechanisms that give rise to an architectural structure that allows for protection from environmental stressors, adequate nutrient and waste flow, and contact for bacteria with other cells and their host (67). We have shown for monospecies *H. pylori* biofilm formation, chemorepulsion from AI-2 is a determinant of spatial organization and dispersal. Given that AI-2 is an important inter-species signaling molecule, we hypothesize that it may play an important role in mixed species biofilm formation as well.

In addition to *H. pylori*, *E. coli* has also been shown to exhibit chemoresponses to AI-2, in this case sensing the quorum signal as a chemoattractant (42). Interestingly, biofilms of a Δ*luxS* strain of *E. coli* were found to be thinner and less dense than their wild-type counterparts (68), consistent with the absence of a self-produced attractant. Furthermore, the same study showed the addition of exogenous AI-2 to Δ*luxS E. coli* biofilms resulted in a partial but significant rescue of biofilm biomass, similar to the partial rescue we observe upon AI-2 addition to Δ*luxS H. pylori*. This suggests that AI-2 may influence spatial organization and adhesion in *E. coli* biofilms in an analogous but opposite way as in *H. pylori* biofilms. *E. coli*'s ecological strategy may be to use AI-2 to locate and persist in the densely colonized colon, whereas *H. pylori* may use AI-2 to

promote dispersal out of individual gastric glands where concentrations of AI-2 are likely to be high. Similar to our observations with *H. pylori*, a *luxS* mutant of *Vibrio cholera* is reported to develop more adherent biofilms (69), implying a possible chemorepulsion response to AI-2.

Given that nearly all biofilms in nature are comprised of many organisms (25), it is interesting to speculate how collective AI-2 production and individual AI-2 perception could organize biofilm structures. High AI-2 producers would serve as foci for those species attracted to AI-2 whereas AI-2 consumers could create permissive microenvironments for organisms averse to high AI-2 concentrations, with organisms of similar AI-2 preferences becoming segregated in the process. More generally, differential chemoresponses to bacterial-produced chemicals could be strong drivers of multispecies biofilm organization, layered upon the existing chemical landscape of the pre-colonized environment, be it a host tissue or an abiotic surface.

If AI-2 is a common chemotactic cue among bacteria, this knowledge could be harnessed for treatment of human infections. A recent report showed that AI-2 production by a colonic commensal, *Ruminococcus obeum*, can promote the resolution of *Vibrio cholera* infection in a gnotobiotic mouse model, through an unknown mechanism (70). We speculate that high AI-2 producing commensals may serve as sources of repulsive cues that drive *Vibrio cholera* from the intestine. In the case of *H. pylori*, broad spread inflammation of gastric tissue throughout the organ is correlated with increased gastric cancer risk (4), presumably due to broader distribution of *H. pylori* in the stomach. It may be possible to manage the spread of *H. pylori* infection by inhibiting the AI-2 chemotaxis

pathway to prevent dispersal of the cells to other areas of the stomach, thus reducing the risk for more severe disease.

## *Methods*

### *H. pylori strains and bacterial culture*

*H. pylori* strain G27 was the primary strain used in this study (71), and it was the wild-type strain from which isogenic mutants were derived. Mutant strains were selected using the appropriate antibiotic media and verified by PCR genotyping. Genetic complementation of disrupted genes was achieved by inserting the full coding region plus predicted promoter sequence of the disrupted gene into the *rdxA* locus (72). The *tlpB* complemention strain replaced the wild type gene at the endogenous locus with a point mutant ($tlpB^{D114N}$) (55) that retains AI-2 chemotaxis but is acid chemotaxis deficient. The *aibA* complemention strain (*aibA**) replaced the wild type gene at the endogenous locus with a copy of the *aibA* gene at the *rdxA* locus. Due to *aibA* being in a potential operon, the *aibB* promoter was inserted upstream of the *aibA* gene. The *aibB* complementation strain (*aibB**) replaced the wild type gene at the endogenous locus with a copy of the *aibB* gene with native putative promoter at the *rdxA* locus. The luxS overproducer strain ($luxS^{OP}$) was constructed by inserting an additional copy of luxS into the *rdxA* locus. Strains were grown on BBL Columbia Agar (BD) plates supplemented with 5% defibrinated horse blood, vancomycin (10 μg/μl), amphotericin B (8 μg/ml), and beta cyclodextrin (0.2% w/v) or in liquid Brucella Broth containing 10% fetal bovine serum (BB10) media in standard conditions, as previously described (56).

The *H. pylori* strain G27MA was used (57) for the microcolony experiments in Figure 5 due to poor colonization by G27 on MDCK cell epithelia. Δ*cheW,* Δ*luxS,* Δ*tlpB,* Δ*cheA,* Δ*aibA,*and Δ*aibB* mutants in G27MA were constructed by deletion of the *cheW*, *luxS*, and *tlpB, cheA, aibA,* and *aibB* coding DNA sequence, respectively, using a PCR based method as previously described (73). The coding DNA sequence of *cheW*, *luxS, cheA, aibA* and *aibB* were replaced with the *aphA* gene (conferring kanamycin resistance). The coding DNA sequence of *tlpB* was replaced with the *cat* gene (conferring chloramphenicol resistance). Mutants were selected on the appropriate antibiotic media and verified by PCR.

*Biofilm imaging*

*H. pylori* cultures were grown in BB10 broth, shaking in microaerobic conditions at 37°C until an $OD_{600}$ of 0.6-0.9. The cultures were diluted back to $1x10^7$ cells $ml^{-1}$. 100 µl of culture was placed onto a clean glass slide (22mm x 22mm) and allowed to incubate in a humidified chamber for 5 days at $37^OC$, 10% $CO_2$ at which point a thick biofilm was readily visible on the air-liquid interface over the surface of the drop. The slides were carefully removed from the incubator and placed onto a $55^OC$ heating block to gently evaporate the media, allowing the biofilm to settle onto the glass slide. The biofilm was fixed with 4% PFA in 1x PBS for 15 minutes, then washed 3 times with 1x PBS. To visualize, one drop of Vectashield hard set with DAPI (Vector Labs) was added to the biofilm and covered with a coverslip. Biofilms were imaged with a 10x lens on a Nikon Eclipse TE2000-U microscope.

*Frac-Lac analysis of biofilm images*

For each slide, a minimum of three images were taken across the entirety of the biofilm. The contrast of the biofilm images was altered in Matlab using the built-in function adapthisteq.m (contrast-limited adaptive histogram equilization- CLAHE) with a ClipLimit parameter of 0.05. The altered images were thresholded using Otsu's method (example in Fig. A2A',B'). The resulting binary images were run through the FracLac plug-in in ImageJ (48, 74) to determine lacunarity with a Box Count analysis of binary images (black background) using a block series with 12 orientation positions and block sizes from 0 pixels to 32% of image. Lacunarity scores were pooled by strain across a minimum of two experiments per strain.

*Biofilm adherence assay*

We used a biofilm adhesion assay previously described (44). *H. pylori* cultures were grown in BB10 to an $OD_{600}$ of 0.6-0.9 and cultures were diluted back to $5x10^7$ cells $ml^{-1}$. 1 ml cultures were added to a 12 well suspension culture plates (Olympus plastics) filled approximately 1/3 full with autoclaved glass frit (Bullseye Glass) to increase the surface area available for cell attachment. Each experiment used 3 or 4 replicate wells filled with the same culture of *H. pylori*. The culture plates were incubated stationary for 2 days at 37°C, 10% $CO_2$. To quantify cells in the planktonic and biofilm populations, 1 ml of 1% crystal violet dye was added to cultures and allowed to incubate for 15 minutes. The liquid was removed via careful aspiration, and cells were spun down for 3 minutes at 13500 rpm and saved as non-adherent cells. The adherent cells that were attached to the sides of the well and the frit were washed three times with 1 ml of 1xPBS. Each wash

was added to the tube of non-adherent cells, spun down, and saved. After washes, the crystal violet in the cells of both the adherent and the non-adherent populations was extracted in 1 ml of 95% ethanol, and spun at 13500 rpm to pellet out cells. The absorbance of the supernatant was then measured using a spectrophotometer at $OD_{595}$. The percent adherence of biofilm cells in the total population of the well was calculated as the absorbance of the adherent population divided by the sum of absorbance of both adherent and non-adherent cells, multiplied by 100.

For experiments adding exogenous AI-2 ((S)-4,5-Dihydroxy-2,3-pentandione, DPD, Omm Scientific), strains were grown as above. The culture was then split into two subcultures, one with AI-2 added to a final concentration of 37 nM and the other treated with an equal volume BB10 as a control. The cultures were added to the glass frit and incubated for two days and analyzed as above. The fraction adherence of cultures with AI-2 addition was compared directly to the control, and was calculated by dividing the average percent adherence of the AI-2 treated cultures by the average percent adherence of the non-treated control.

For experiments where AI-2 was added to replacement media, the strains were grown up as above. After 48 hours the liquid media was removed by pipette from each well. To wash the biofilm cells, 1 ml of BB10 was gently added to each well and removed. 1 ml of media, either with or without the addition of AI-2 to a final concentration of 37 nM, was added back to the wells and incubated for 24 hours. The crystal violet assay was used to quantify the proportion of cells in the biofilm separately from the proportion of cells in

the planktonic media. The change in biofilm size or planktonic cell number after addition of AI-2 was calculated by finding the difference in $Abs_{595}$ of cultures with AI-2 from $Abs_{595}$ of the BB10 control.

*Identification of putative periplasmic binding proteins in H. pylori G27*

Proteins annotated as being "transport and binding proteins" in *H. pylori* strain J99 were identified using The Institute for Genomic Research (TIGR). The seven proteins were analyzed using Basic Local Alignment Search Tool for proteins (BLASTp) for homology to other known periplasmic binding proteins. Of the seven, five protein candidates remained. The corresponding proteins and genes in *H. pylori* G27 were identified using BLASTp and were further characterized for roles in AI-2 chemotaxis.

*Chemotaxis response assay*

As previously described (20), *H. pylori* were inoculated into liquid BB10 media from plate and grown shaking to an $OD_{600}$ of 0.7-0.9. Cultures chosen to assay had at least 60% of cells motile and minimal clumping. An 8 µl sample was spotted onto a glass slide and covered with a coverslip (22mm x 22mm). The coverslip was sealed on 3 sides with clear nail polish. 8 µl of treatment (BB10, 100 mM HCl in BB10, or 100 µM synthetic AI-2 in BB10) was added to the side of coverslip not sealed. After approximately 5-10 minutes, the culture was imaged at 10x through a ×40 phase filter on Leica DMIL microscope. The formation of a barrier indicated a response to treatment. Representative images were taken of the barrier, or in similar locations on the slide in conditions with no barrier formation.

*Protein purification and AI-2 binding assay*

Assessment of the AI-2 binding ability of proteins were based on previous methods (53, 54). LsrB (kindly provided by Stephen T. Miller, Swarthmore College, Swathmore, PA) was cloned into the pGex-4T-1 expression vector. The periplasmic portion of the *tlpB* gene (coding for TlpB residues 33-211) were cloned into a pGex-4T-1 expression vector. *aibA* and *aibB* genes were cloned lacking the periplasmic targeting sequence (*aibA* lacking the coding region for amino acids 1-22, *aibB* lacking the coding region for amino acids 1-24) into a pGex-6P-1 expression vector (GE Healthcare). The plasmids were transformed into BL21 *E. coli* for protein expression. Protein purification was achieved using a Glutathione Sepharose 4B column (GE Healthcare) following the recommended protocol. The GST tag was left on the purified proteins after we determined GST alone did not show AI-2 binding activity (data not shown). The GST tag was cleaved from AibB because of apparent partial spontaneous cleavage of the GST tag during purification. GST cleavage was achieved after elution of AibB from the column by adding 1 unit of PreScission Protease enzyme and incubated overnight at 4°C as described (GE Healthcare). Purified proteins were dialyzed into a storage buffer of 300 mM NaCl, 10 μM Tris (pH 8) and 5 μM 2- mercaptoethanol, concentrated with a VivaSpin-20 filter (GE Healthcare), and stored at -80°C.

For the protein-AI-2 binding assay, all purified proteins were normalized by dilution into assay buffer (300 mM NaCl, 10 mM sodium phosphate pH 7) to a concentration of 6 mg $ml^{-1}$ as quantified by NanoDrop-1000 spectrophotometer (Thermo-Fisher Scientific). 200

µl protein was incubated with 100 µl of 1 mM synthetic AI-2 diluted into assay buffer at 4°C for 120 minutes. The sample was loaded onto a Sepharose G25 fine column (Sigma Aldrich). The column was washed with 4 x 200 µl volumes of assay buffer and the eluate was collected. Protein eluted was quantified by direct application of the sample to the Nanodrop and concentrated to 100 uL using Amicon Ultra 10K membrane centrifugal filter. Retentate was incubated in a 55°C water bath for 10 minutes to denature the protein and release any bound AI-2 into the supernatant. The sample was centrifuged at 14,000 rpm for 2 minutes to pellet protein.

The supernatant was directly used in *Vibrio harveyi* luminescence assay to test for AI-2 levels as previously described (56). Briefly, an overnight culture of *V. harveyi* was diluted 1:5000 in fresh AB medium (300 mM NaCl, 50 mM MgSO4, 2% w/v casamino acids, 10 mM potassium phosphate pH 7, 1 mM L-arginine, 1% w/v glycerol). 90 µl of diluted *V. harveyi* culture was added to 10 µl of protein supernatant and put into a 96-well plate in triplicate. Levels of luminescence were measured on a SpectraMax M5e plate reader (Molecular Devices) each hour over the course of 6 hours with incubation on a shaker at 30°C in between measurements. Relative luminescence units (RLUs) for each sample were taken at the time point where there was the largest difference between an exogenous AI-2 positive control and a buffer negative control, and normalized as a percent of the exogenous AI-2 positive control.

*Cell culture*

Madin-Darby Canine Kidney II (MDCK) cells (kindly provided by W. James Nelson,

Stanford University, Stanford, CA) (75) were grown in DMEM (Gibco) containing 10% FBS (Gibco) at 37°C in a 5% $CO_2$ atmosphere. Polarized MDCK monolayers were generated as previously described (18). Briefly, about a half million cells were seeded onto 12 mm, 0.4 μm-pore polycarbonate tissue culture inserts (Transwell filters; Corning Costar). One day after seeding, the apical medium was changed to DMEM and the basal medium was changed to DMEM + 10% FBS. For four subsequent days, the basal medium was replaced daily with fresh DMEM + 10% FBS while the apical medium was unchanged. On the fifth day post seeding, the monolayers were ready for use.

*H. pylori infection of polarized MDCK monolayers*

The basal media of polarized monolayers were replaced with coculture medium (DMEM + 10% FBS + 10% Brucella broth). The apical surfaces of polarized monolayers were washed 3 times with DMEM. Then 500 μl of a bacterial culture at $OD_{600}$ of 0.2 (~$10^8$ colony forming units (CFU)/ml) was added to the apical side of the monolayer and allowed to infect for 5 minutes at 37°C in a 5% $CO_2$ atmosphere. Infected monolayers were washed 4 times with fresh DMEM to remove non-adherent bacteria. DMEM was added back to the apical side of the monolayer, and the cells were kept at 37°C in a 5% $CO_2$ atmosphere. Each day for 3 days, the basal medium was replaced with fresh coculture medium, the apical chamber was sampled for CFU, and the monolayers were washed 4 times with DMEM before fresh DMEM was added back.

*Confocal immunofluorescence microscopy and antibodies*

At terminal time points, samples were fixed and processed for confocal immunofluorescence as previously described (76). Chicken anti-*Hp* G27MA (57) was used at 1:500 dilution and mouse anti-ZO-1 was used at 1:100. *H. pylori* was detected using a goat anti-chicken 594 secondary antibody, and ZO-1 was detected using a goat anti-mouse 488 secondary antibody. DAPI (Invitrogen) was also used to stain for cell nuclei. Samples were imaged at 40x with a Zeiss LSM 700 confocal microscope, and extended focus images of z-stacks were analyzed via a custom MATLAB script.

*Statistical analysis*

All data analysis was performed using R (77) unless otherwise specified. A value of $p=0.05$ was used as a cut off to determine significance. All experiments have a minimum of 3 replicates unless otherwise specified.

For data analysis of biofilm lacunarity (Fig. 1F, 3H), statistical analysis was performed in GraphPad Prism (version 6.03 for Windows GraphPad Software, San Diego California USA, www.graphpad.com) by pooling lacunarity scores from individual images over different experiments and compared to WT using a Student's T-test. For percent adherence (Fig. 1H, Fig. 3I), percent adherence values from multiple experiments were pooled, arcsine-square-root-transformed, and assessed with a one-way ANOVA and Tukey HSD test against WT. To determine significance of increased RLU (Fig. 2B), the percent RLU from replicate experiments were pooled and compared to the buffer negative control using a Student's T-test to determine significance. For analysis of

change with AI-2 addition (Fig. 4A), the difference in percent adherence for each experiment were pooled and tested against the null hypothesis of $\mu=0$ (no change) using a Student's T-test. For analysis of fraction change with AI-2 addition to replacement media (Fig. 4B), the values were pooled from multiple experiments and tested against the null hypothesis of $\mu=1$ (no change) using a Student's T-test. To calculate estimated number of attached bacteria on MDCK cells (Fig. 5D), the images of *H. pylori* microcolony cells were quantified using MAT-LAB to measure the size of microcolonies in pixels. The number of cells in the microcolonies was estimated by dividing the number of pixels in the microcolony by 20 (the empirically determined number of pixels for a single *H. pylori* cell). The number of *H. pylori* cells in the field of view was extrapolated to estimate the number of attached *H. pylori* cells in the entire transwell, and was averaged among the triplicate fields of view taken in the same well. Significance of 3 day attachment from 5 day attachment was achieved by performing a student's T-test using GraphPad Prism within strains. To compare average microcolony size (Fig. 5E), the average microcolony sizes at 3 days were pooled and compared to WT with a one-way analysis of variance with Tukey's test using GraphPad Prism.

# CHAPTER III

# INVOLVEMENT OF AIBA AND AIBB PROTEINS IN THE MECHANISM OF AUTOINDUCER-2 SENSING

## *Introduction*

In most chemosensory systems, the methyl-accepting chemotaxis protein (MCP) receptor is able to bind the ligand directly and relay the signal to the Che proteins inside the cell. A few systems are known that use periplasmic binding proteins (PBPs) (also known as ligand binding proteins) that bind chemoeffector molecules and relay the signal to the MCP receptors (52). The other known AI-2 chemotaxis pathway in *E. coli* follows this mechanism, with the LsrB PBP hypothetically interacting with the MCP receptor Tsr (42). Our observations that AibA and AibB are both able to bind AI-2 independently and are both necessary for AI-2 chemotaxis in *H. pylori* suggest a unique molecular model for chemotaxis. This motivated us to further explore the features of these previously uncharacterized proteins that contribute to the molecular mechanism of AI-2 chemotaxis.

We modeled the structures of the AibA and AibB proteins to better understand their characteristics and generate hypotheses about important features of these proteins. To do this, we used the Iterative Threading ASSEmbly Refinement (I-TASSER) computer algorithm to predict tertiary structures of AibA and AibB (78). We inputted the amino acid sequences of AibA and AibB into the I-TASSER program, which generated a template model using known structures of proteins in the protein data bank using a Local Meta-Threading Server (LOMETS), which was further refined into a full model of protein structure through template fragment assembly. Comparing these generated models to known structures of proteins with ligands bound allowed us to make

predictions of putative binding pockets and residues important for ligand binding, and revealed interesting conserved structural features of these proteins that may suggest a shared protein binding partner.

### *Predicted Models of AibA and AibB Tertiary Structures*

The AibA amino acid sequence lacking the periplasmic targeting sequence (first 43 amino acids) was submitted to the I-TASSER server, which used 10 templates from 4 protein sequences (Protein Data Bank (PDB) ID: 3tpaA, 3m8u, 1dpeA, and 4qfk) to generate template models. The top sequence was PDB 3tpA, which is a homologous protein called HbpA2 in *Haemophilus parasuis* that has approximately 40% identity at the amino acid sequence level. These template structural models of AibA were then compared to crystal structures if other homologous proteins with ligands bound to determine the most likely structural model and to identify putative binding pockets within AibA. The model of AibA generated with the highest confidence (C-score = 1.78) was most similar to the protein GbpA from *H. parasuis* (PDB: 3M8U) with 38% sequence identity (Figure 6). AibA is predicted to be structurally similar to many type-2 PBPs, which typically bind their ligand in the cleft between two globular subdomains (79). Consistent with this observation, there is a predicted binding pocket in AibA in a similar location to the binding pocket of the type-2 PBP GbpA. Using the structure of GbpA with ligand bound (glutathione di-sulfide), we can predict which residues in the binding pocket of AibA are likely to be important for AI-2 binding. We identified two serines, S521 and S538 that have side chains in the binding pocket that are primed for hydrogen bonding to a small molecule such as AI-2 (Figure 6, blue side chains). We hypothesize

that mutating these residues to disrupt potential interactions with ligands in the binding pocket would render the protein unable to bind AI-2, and would abolish the ability of *H. pylori* with these mutations to respond chemotactically to AI-2.

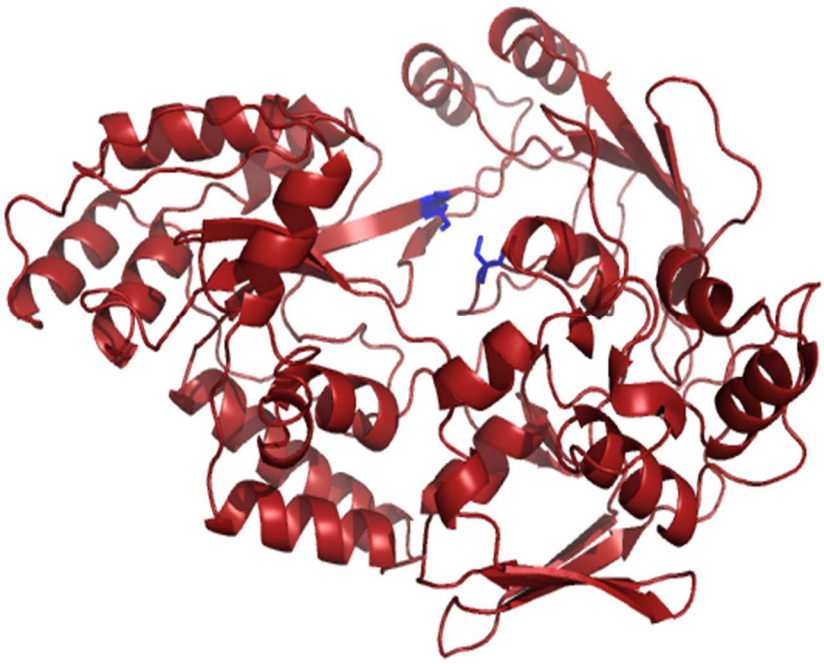

**Figure 6: Model of AibA tertiary structure.** I-TASSER generated model of AibA protein, based on structural similarity to GbpA from *H. parasuis* (PDB: 3M8U). Blue side chains correspond to serine residues S521 and S538 that are predicted to be important for ligand (AI-2) binding.

We modeled the structure of AibB in a similar way as AibA using the I-TASSER server. Within the top 10 templates for threading with 3 different protein sequences (PDB 1ATG, 3CIJ, and 4KD5), the top sequence being for the ModA protein from *Azotobacter vinelandii* (36% sequence identity, PDB: 1ATG). The top model with highest confidence score had high structural similarity to the ModA protein from *E. coli* (PDB: 1WOD, 36% identity). The predicted structure for AibB has a high confidence score (C= 1.32), and

appears to be structurally similar to other type-2 PBPs (Figure 7). Overlay of the ModA structure with ligand bound (molybdate ion) onto the predicted structure of AibB reveals a putative binding site in AibB. We hypothesize that two serines, S59 and S163, are important for AI-2 binding in AibB given the proximity of the side chains in the putative binding pocket and the ability to establish hydrogen bonds to a small molecule like AI-2 (Figure 7, blue side chains). As with our hypothesis for the resides in AibA, we predict that mutating these serines in AibB will disrupt AI-2 binding and render the *H. pylori* cells that harbor these mutations unable to respond to AI-2. Future work will test these mutations both *in vitro* for protein-AI-2 binding, as well as *in vivo* in the barrier chemotaxis and biofilm assays.

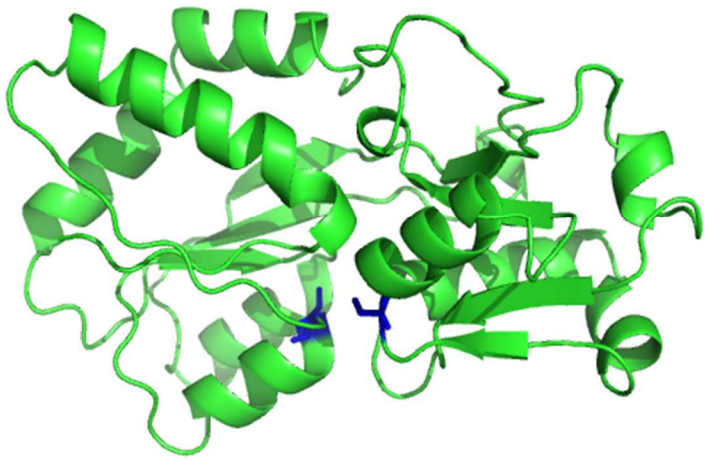

**Figure 7: Model of AibB tertiary structure.** I-TASSER generated model of AibA protein, based on structural similarity to GbpA from *E. coli* (PDB: 1WOD). Blue side chains correspond to serine residues S59 and S163 that are predicted to be important for ligand (AI-2) binding.

PBPs participate in many important functions in the cell. PBPs are known to participate in chemoreception, but also in small molecule transport through the

membranes and sensory transduction pathways (80). It is not uncommon for a single periplasmic binding protein to have multiple functions in the cell (52). PBPs have ligand-binding sites that adapt to bind a chemically diverse array of ligands (81), which allow them to mediate various functions. It is not surprising that AibA and AibB share such high homology to proteins in other systems with different identified functions, but for AibA and AibB, AI-2 binding and role in chemotaxis is the first function demonstrated for these proteins in *H. pylori*.

### *Amino Acid Sequence Alignment Reveals Conserved Peptide Sequence in AibA and AibB Proteins*

As previously described, AibA and AibB are both Class 2 PBPs, but belong to different clusters within the classes and share little sequence homology (21% sequence identity, Figure A4) (82). I performed an amino acid sequence alignment of AibA and AibB using the ClustalW2 Multiple Sequence Alignment program (Figure 8A). As expected, there is little sequence conservation between the two proteins, but there are areas with homology. The first area of homology between these proteins is within the first approximately 20 amino acids at the N-terminal ends of the proteins that resemble a periplasmic targeting sequence. A second area of homology between AibA and AibB is a conserved 14 amino acid region towards the C-terminal end of both proteins that corresponds to surface exposed predicted alpha helices in both AibA and AibB (Figure 8B,C).

A

```
AibA            MNNVFVKGLFFFLLLFGSFLKASENPNAALNPSKENVSVEEQKRFGGVLVFARGADGSSM 60
AibB            MKNTFKAFAFLIVFFSSALLAQDLKIAAAANLTRALKALVK--------EFQKEHPKDAI 52
                *:*.*    *::::: .::*  . :  ** * ::   :: :         * :    .::

AibA            DPALVTDGESYVATGNIYDTLVQFKYGTTEIEPALATSWDISPDGLVYTFHLRKGVYFHQ 120
AibB            S-------ISFNSSGKLYAQIIQN-----------------APFDLFIAADITRPKKLYD 88
                .        *: ::*::*  ::*                   :* .*. : .: :   :::

AibA            TKYWNKKVEFSAKDVLFSFERQMDKAKRYYSPGAKSYKYWEGMGMSHIIKSIEALDDYTI 180
AibB            EKITPFKEEVYAKGVLVLWS---------------------------------------- 108
                 *    * *. **.**. :.

AibA            RFTLNGPEAPFLANLGMDFLSILSKDYADYLEQNNKKDELAKKPVGTGPFKFFLWNKDEK 240
AibB            ------------ENLKMDSLEILKDPKIKRIAMANPK----LAPYGKASMEVLEN----- 147
                           ** ** *.**..   . :   * *      * *...::.:

AibA            IILLKNQDYWGPKAYLDKVVVRTIPNSSTRALALRTGEIMLMTGPNLNEVEQLEKLPNIV 300
AibB            ---LKLTPSLKSKIIYGASISQAHQFVATKNAQIGFGALSLMD-------KKDKNLSYFI 197
                   **      .*   .  : ::    :*:   :  * : **        :: ::*. ::

AibA            VDKSPGLIANWLSLNTQKKYFNNPLVRLAINHAINVDDYIKVIYEGFAQKMVNPFPPTIW 360
AibB            IDKA----------------LYNPIEQALIITKNGANNPLAKVFKDFLFSP--------- 232
                :**:                : **: :  *    ..:: :  :::.*  .

AibA            GYNYNIKPYEYDLKKAKELLKQAGYPNGFKTTIFTTSTRNPKGAVFIQASLAKIGIDVKI 420
AibB            --------------KARAIFKEYGYIVD-------------------------------- 246
                             **: ::*: **  .

AibA            EVYEWGAYLKRTGLGEHEMAFAGWMADIADPDNFLYTLWSKQAASAIPTQNGSFYKSDAF 480
AibB            ------------------------------------------------------------

AibA            SDLLIKAKRVSDQKEREALYLKAQEIIHKDAPYVPLAYPYSVVPHLSKVKGYKTTGVSVN 540
AibB            ------------------------------------------------------------

AibA            RFFKVYLEK 549
AibB            ---------
```

B

C

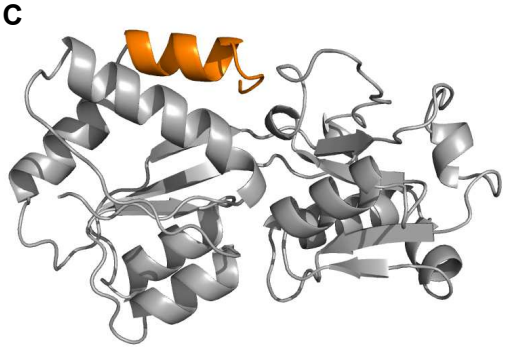

**Figure 8: Shared features between AibA and AibB proteins.** (A) ClustalW2 generated alignment of amino acid sequence similarity between AibA and AibB. Numbers at the end of each row indicate residue position number of the last residue in the row. Asterisks indicate positions that have a single, full conserved residue; colons indicate positions that have residues that have strongly similar properties; periods indicate positions that have residues that have weakly similar properties. Residues colored red are small, hydrophobic; residues colored blue are acidic; residues colored magenta are basic; residues colored green are hydroxyl, sulfhydryl, amine, or glycine. A conserved 14-amino acid region at the C-terminal ends of both proteins is colored and represented in the modeled structures in orange for both AibA (B) and AibB (C).

We hypothesize this exposed alpha helix may be functionally relevant in these proteins, given their position within the proteins as surface exposed alpha helices. Surface exposed alpha helices can often be important for mediating protein-protein interactions (83), and this conserved helix may suggest a shared binding partner for both AibA and AibB. One likely candidate for a shared binding partner would be the chemoreceptor TlpB, since all three proteins are required for AI-2 chemotaxis in *H. pylori*. To test this hypothesis, I propose to mutate residues in the predicted exposed alpha helix to change the charges of some of the residues in this region and test if these are necessary for AI-2 chemotaxis. Altering the positive charged residues in these alpha helices to negative charged residues such as glutamic acid (AibA: K374E, K377E, K381E; AibB: K233E, R235E, K239E; Figure 8A in magenta) could disrupt the electrostatic interactions this alpha helix may have with the binding partner and result in lack of ability of *H. pylori* to respond to AI-2 chemotactically, which can be tested using the barrier or biofilm chemotaxis assays.

*Proposed Model of AibA and AibB in the Mechanism of AI-2 Chemotaxis*

The requirement of AibA, AibB, and TlpB for AI-2 chemotaxis in *H. pylori* is a unique variation of a common chemotaxis mechanism. There are many examples of chemotaxis mechanisms that require a PBP and a chemoreceptor to sense ligands (52, 84). The only other known AI-2 chemotaxis mechanism is in the enteric bacteria *Escherichia coli* that perceive AI-2 as a chemoattractant (42). The PBP LsrB has known AI-2 binding capabilities and is hypothesized to interact with the chemoreceptor Tsr. I hypothesize a similar mechanism in *H. pylori* whereby AibA and AibB interact with

TlpB to promote AI-2 chemorepulsion (Figure 9). I cannot predict whether or not AibA and AibB physically interact; I have shown that both AibA and AibB are both required for AI-2 chemotaxis, which might suggest potential binding between these two proteins. Additionally, I have shown that two copies of *aibB* is not sufficient to rescue the loss of *aibA* (data not shown), which suggests that overexpression of one protein is not sufficient to rescue the loss of the other. This may support the hypothesis that AibA and AibB may be forming a heterodimer in the periplasm. However, I have also shown that both proteins are able to bind AI-2 independently of one another, which suggests that binding between AibA and AibB may not be necessary. To fully elucidate this model, interactions between AibA and AibB would need to be tested either with purified protein components or through a co-immunoprecipitation.

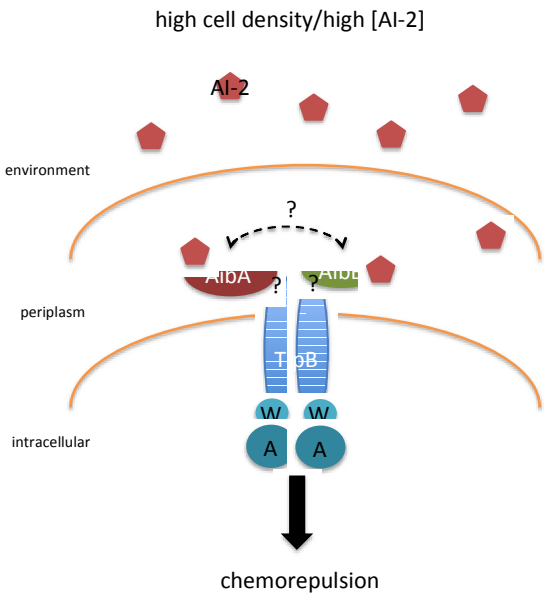


**Figure 9: Proposed model for the mechanism of AI-2 chemotaxis in *H. pylori*.** At high cell density, high amounts of AI-2 are in the environment and bind to AibA and AibB proteins, which may interact with the chemoreceptor TlpB to promote chemorepulsion. CheA and CheW proteins are denoted by A and W respectively. Hypothetical interaction between AibA and AibB illustrated with dotted double-headed arrow; hypothetical interaction between AibA or AibB with TlpB illustrated with question marks.

Direct interactions between proteins in the chemosensory pathway are challenging to observe. For example, while both LsrB and Tsr are required for the AI-2 chemotaxis response in *E. coli*, a direct interaction has never been explicitly demonstrated. The one example of PBP-chemoreceptor interaction is the Maltose Binding Protein (MBP) – Tar chemotaxis system in *E. coli* (85, 86). This interaction was deemed challenging for biochemical analysis due to the low affinity of MBP to the Tar chemoreceptor (estimated at 250 μM from *in vivo* measurements) (87). I hypothesize that the interactions between AibA, AibB, and TlpB, if present, would also be low affinity, transient interactions. A potential benefit of having transient interactions of proteins in a chemotaxis sensory pathway would be to not over amplify the signal present in the environment. If proteins in the chemotaxis system bound each other with high affinity when ligand was present, this would amplify the signal to the flagellar motor and decrease the sensitivity of chemotaxis proteins to concentrations of chemicals in the environment. A method being used more frequently in the bacterial chemotaxis field for detecting these more transient interactions is fluorescence resonance energy transfer (FRET) and bioluminescence resonance energy transfer (BRET) (88). Further elucidating the critical structural features of AibA and AibB would pave the way for the use of these more sensitive methods for detecting potential interactions between AibA and AibB, and interactions with the chemoreceptor TlpB.

The requirement of both AibA and AibB to sense AI-2 is unique mechanism within known chemotaxis pathways. To my knowledge, this is the first chemotaxis mechanism that requires two PBPs to sense the same ligand. This brings up the question as to how this unique mechanism arose in *H. pylori*, and what benefit this has for the

organism. Given the lack of sequence homology between AibA and AibB, I can conclude that these are functional homologs but are not paralogs. Through bioinformatics analysis, AibA and AibB are both highly conserved within the *H. pylori* species, suggesting that there is evolutionary selection for these proteins. The two functionally similar but sequence dissimilar proteins likely did not arise from a gene duplication event during *H. pylori* evolution. *H. pylori* is a naturally competent bacterium (89), so it is possible that the second gene was acquired from another organism (perhaps for the advantage of a yet to be determined other function) and developed the capability of AI-2 binding. There are examples of organisms adapting to multiple copies of functionally similar proteins (90) in which, over time, the proteins acquire degenerative mutations that render them unable to perform the function alone and require the other gene/protein, thus providing strong selective pressure to keep both functionally homologous proteins. AI-2 sensing has been shown to be important in many bacterial species (22), so a hypothesis could be that *H. pylori* adapted these proteins for use in AI-2 sensing due to a competitive advantage that quorum sensing and AI-2 chemotaxis have for the bacterium. The ability for cells to not only be able to sense population size of bacteria within their immediate vicinity, but to be able to respond through directed motility to areas of less population density would increase their access to nutrients and different habitats within their environment.

## *Methods*

### *I-TASSER and Modeling of PBP structure*

DNA sequences of *aibA* and *aibB* were collected from the UCSB Genome Browser (91). DNA sequences were converted to amino acid sequences using the ExPASy Translate

Tool. These sequences were submitted to the I-TASSER server with the periplasmic targeting sequence removed (AibA beginning at amino acid 44, AibB beginning at amino acid 23). The server provided the top 5 most confident predictions for tertiary structure for AibA and AibB, and the models with the highest confidence score (C-score) were chosen as the most likely model for protein structures (AibA c-score: 1.78; AibB c-score: 1.32). The models were imported for image generation into Pymol for Windows (Pymol V.1.3).

*Bioinformatic analysis of AibA and AibB proteins*

Amino acid sequences for AibA and AibB were analyzed for putative domains using NCBI BLASTp by searching within the Protein Data Bank. Sequence alignment between AibA and AibB was performed and analyzed using the ClustalW2 Multiple Sequence Alignment tool. Conservation of *aibA* and *aibB* genes was determined by using NCBI BLASTn and searching the genomes under the organism *Helicobacter* (taxid:209).

# CHAPTER IV

# DISCUSSION

## *Implications of AI-2 Chemotaxis for Treatment Strategies of H. pylori Infection*

The findings described in the previous chapters have broad implications that can be used for evaluating current treatment strategies, as well as developing novel treatment strategies in the treatment or modulation of *H. pylori* infection. As infection with *H. pylori* still remains an important risk factor for the development of gastric cancer, effective treatments are critical for prevention of disease.

Antibiotics, which have been miracle drugs in the treatment of bacterial infections, are becoming less effective as the acquisition of antibiotic resistance is increasing. The development of new antibiotics is difficult because bacteria are able to evolve resistance to antibiotics due to the high selective pressure antibiotics put on them. Thus, there is a demand for the development of novel antimicrobial treatments that are less likely to promote resistance in bacteria, which is gaining increased recognition. More than $650 million across the National Institutes of Health (NIH) and the Biomedical Advanced Research and Development Authority (BARDA) has been allocated in the coming year to significantly expand American investments in the development of novel antibacterial treatments (92).

The current treatments for *H. pylori* infection include proton-pump inhibitors and at least two antibiotics to eradicate *H. pylori* infection including amoxicillin, clarithromycin, and metronidazole. This therapy is becoming less effective due to increased antibiotic resistance in *H. pylori*. The treatment regiment of a proton-pump inhibitor and two antibiotics can last up to 14 days and cause unpleasant side effects. This

contributes to poor patient compliance, which decreases efficacy of the treatment and can contribute to the growing problem of antibiotic resistance (7, 93). The increase in clarithromycin resistance since the late 1990s is correlated with a decrease in eradication efficiency of *H. pylori* treatments: from > 90% effective to a more recent eradication efficiency of close to 75% (94). To combat this, treatments are incorporating metronidazole more often, which was effective against clarithromycin resistant strains of *H. pylori*, but now is also becoming less effective due to an increase in metronidazole resistant *H. pylori* in many areas in the world, in some areas up to ~40% (7).

In addition to antibiotic resistance, the effectiveness of antibiotics depends on many factors, including dose and exposure of cells to the molecules. Cells within biofilms are known in many systems, including many medically relevant bacteria, to be more resistant to antibiotics than planktonic cells (24, 28, 31). I tested this in *H. pylori* by growing wild type cultures in plastic wells on glass frit for 48 hours as described previously (Chapter II, methods), then adding varying concentration of amoxicillin from 0 to 2.5 μg/mL. After a 24-hour incubation of cells with the antibiotic, I used the crystal violet assay as previously described to quantify the number of planktonic and biofilm cells separately (Figure 10). I observed that the number of planktonic cells decreased significantly in a dose dependent manner with increasing concentrations of amoxicillin. Conversely, the presence of amoxicillin did not change the number of biofilm cells. This suggests that similar to what has been observed in other systems, *H. pylori* cells in the biofilm are more resistant to antibiotic treatment than planktonic cells.

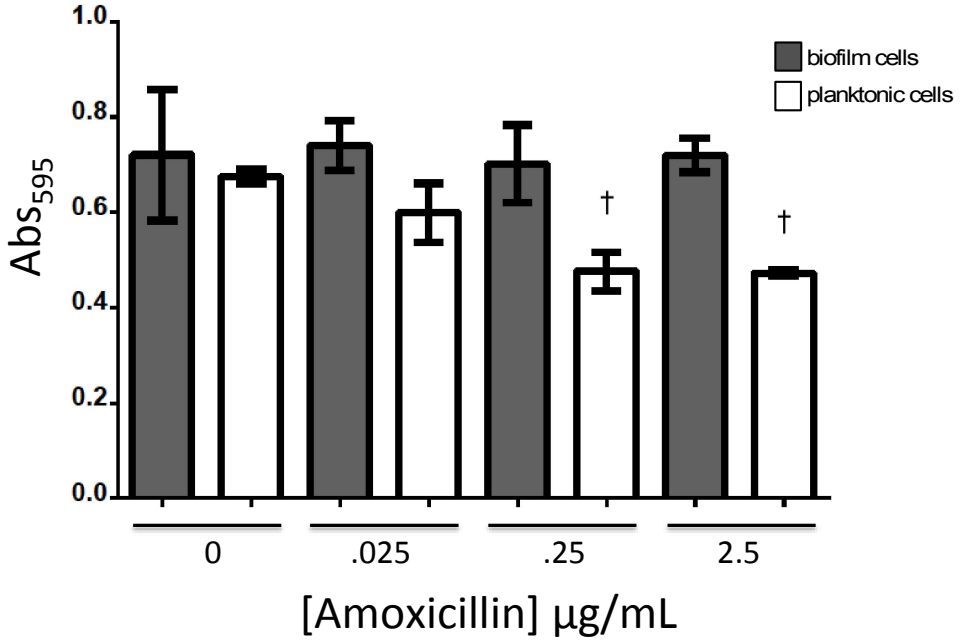


**Figure 10: Effect of amoxicillin treatment on *H. pylori* biofilm and planktonic cell growth.** Biofilm and planktonic cells were quantified 24 hours post amoxicillin treatment using the crystal violet assay. Error bars represent the standard error of the mean for triplicate treatment wells.

As I have demonstrated in this work, both the proportion of cells in biofilms as well as the spatial organization of cells within biofilms is dependent on AI-2 chemotaxis. Given that cells in biofilms are less susceptible to amoxicillin treatment, I would predict that Δ*luxS* or AI-2 chemotactic deficient mutants would have increased protection from amoxicillin because a greater proportion of cells in the population are found in biofilms. One way to increase the effectiveness of an antibiotic treatment may be to induce dispersal of *H. pylori* cells out of the protective biofilms. Designing a drug to induce chemorepulsion and dispersal of *H. pylori* cells out of the biofilms would make them more susceptible to the antibiotic treatment and could be given concurrently with current treatments to improve eradication efficiency.

It is also possible that the spatial organization of cells in biofilms may contribute to the effectiveness of antibiotic treatment. Cells within biofilms secrete molecules to

form the exopolysaccharide (EPS) matrix that help protect them from environmental challenges by limiting diffusion of molecules within the biofilm community (95). Alterations in the spatial organization of cells within the biofilm may change the structure of the EPS matrix, which may have beneficial or detrimental consequences for the cells in the biofilm by changing the permeability of antibiotic molecules through the EPS matrix. An alternative hypothesis to my first prediction that Δ*luxS* or AI-2 chemotactic deficient mutants may have an advantage in protection from antibiotics due to a greater portion of the population residing in biofilms, would be that the alterations in spatial organization I observed may lead to detrimental defects in EPS organization that may actually make the cells more susceptible to antibiotic treatment. A better understanding of the functional consequences of altered spatial organization and adherence observed in *H. pylori* as a result of AI-2 chemotaxis, would inform therapeutic strategies in infection treatment.

One emerging target for antimicrobial therapies is targeting quorum sensing (96–98). This is a promising field of research, because quorum sensing is not necessary for the bacteria to survive; thus, there is less selective pressure for the bacteria to evolve resistance to the antimicrobial treatment (96). Given that quorum sensing modulating drugs would not eliminate the infection, they instead focus on modulating bacterial cell processes and behaviors to something more favorable for the host. This gives an opportunity for the host to either eliminate the bacteria through immune processes, or live with the bacteria in a way that doesn't elicit disease by inhibiting expression of virulence genes by the bacteria or inhibiting biofilm formation (99, 100).

In the case of *H. pylori* infection, it may be beneficial to manage the infection without eradicating it. *H. pylori* has been identified as a pathogen due to it being a causative agent of stomach diseases, however infection with *H. pylori* has also been correlated with a decreased incidence of esophageal cancer in humans, and shown to have a protective effect from asthma in animal models (101, 102). Thus, maintaining an infection with *H. pylori* while minimizing disease risk could offer the most protection of the host from disease.

The research into quorum sensing targeting anti-microbial drugs typically focuses on the gene regulation aspects of quorum sensing. My work would suggest that targeting the chemotaxis aspect of quorum sensing could also be an effective strategy for modulating bacterial behaviors that influence their interactions with the host. Designing a small molecule to modify AI-2 could prevent AI-2 signaling in *H.* pylori. However, given that AI-2 is an inter-species signaling molecule, targeting the AI-2 molecule itself could have more pleotropic effects since it could alter other behaviors in other bacteria. An alternative approach would be to modify the AI-2 binding pocket of AibA and AibB proteins, which would have more specificity to *H. pylori.* Doing so would serve to disrupt AI-2 binding, and could generate an AI-2 "blind" phenotype. I would predict that doing this would promote bacterial behaviors similar to AI-2 chemotactic null mutants, such as decreased in biofilm spatial heterogeneity and decreased dispersal from biofilms. Decreased dispersal may serve to decrease the extent of colonization throughout the stomach and sequester the *H. pylori* infection to the atrium within the gastric glands. Since dispersal is more correlated with severe stomach disease, the hope would be that minimizing dispersal would minimize the host's risk for developing more severe disease.

Although future studies are necessary to fully demonstrate the influence of AI-2 chemotaxis for *H. pylori*, my work has contributed to the understanding of mechanisms that influence the spatial organization of *H. pylori* within their environment. More broadly, I have uncovered a timescale of AI-2 signaling that is much more rapid than the canonical mechanism for AI-2 regulation of gene expression, which may lead to further elucidation of AI-2 sensing and chemotaxis in other bacteria. This will aid in future work in other bacterial systems that will consider chemotaxis to endogenously produced molecules as an important determinant in cellular behaviors that modulate the interactions of bacterial cells with their host and environment.

## *Methods*

### *Effect of antibiotic treatment on biofilm and planktonic cells*

Cells were grown as previously described (Chapter II, Methods, Biofilm adherence assay) and cultured in plastic wells with glass frit for 48 hours. After 48 hours, 50 µL of amoxicillin (VWR International) diluted in BB10 was gently added to the wells to a final concentration of 0 to 2.5 µg/mL amoxicillin with triplicate wells per condition. Cultures were incubated for another 24 hours prior to cell quantification via crystal violet assay as previously described.

# APPENDIX

## SUPPLEMENTAL FIGURES AND METHODS

The following figures and methods correspond to supplemental material for Chapter II and were chosen to be included in the appendix rather than within the main chapter due to the information being helpful, but not critical for evaluating the content in that chapter.

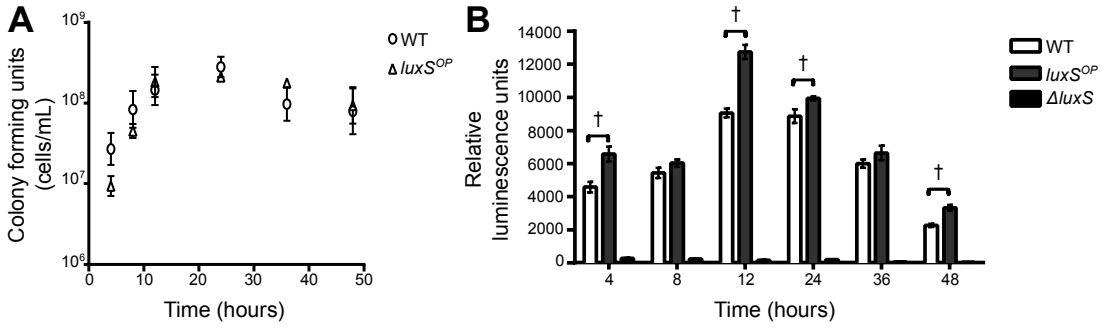


**Figure A1: Relative endogenous levels of AI-2 in *H. pylori* cell free supernatant.** (A) A representative experiment observing CFUs of shaking cultures over time for WT and *luxS*$^{OP}$ strains. Error bars represent the standard deviation of duplicate cell count measurements. (B) Relative luminescence units from *V. harveyi* bioluminescence assay for cell free supernatant collected over time for WT and *luxS*$^{OP}$ strains. Cell free supernatant also collected from Δ*luxS* as a negative control. Error bars represent the standard deviation of duplicate luminescence measurements. Daggers indicate significant increase ($p<0.05$) of *luxS*$^{OP}$ from WT using a Student's T-test.

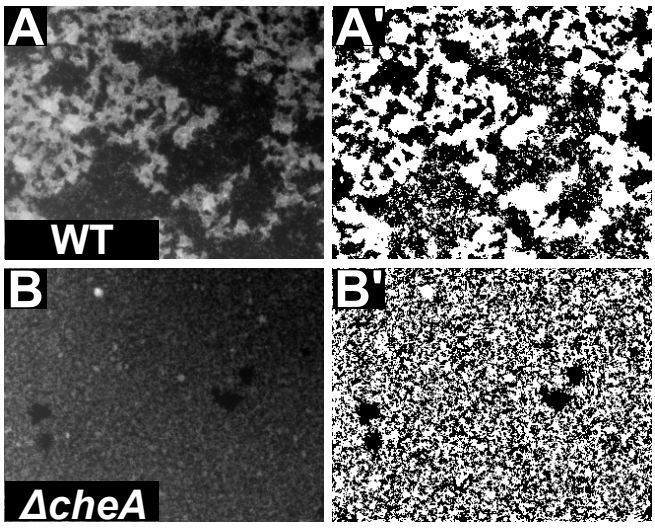


**Figure A2: Thresholding images for lacunarity measurement.** Example biofilm images of WT (A) and Δ*cheA* (B) biofilms with corresponding thresholded images (A', B') used for lacunarity scoring (Fig. 1F, 3G).

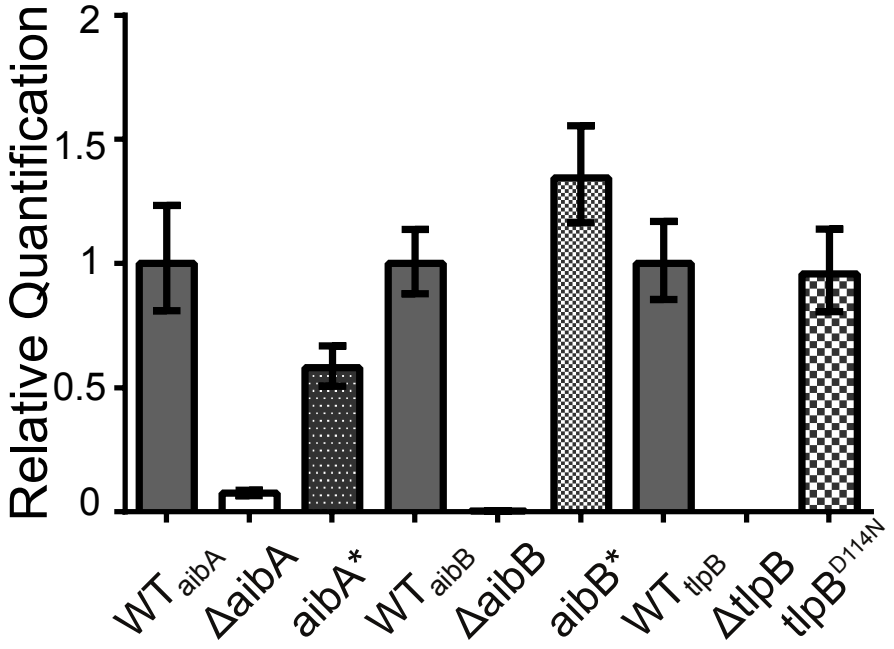


**Figure A3: Relative quantification of transcript levels of *aibA, aibB* and *tlpB* genes.** qRT-PCR analysis of cDNA from WT, mutant, and complement strains. Amplification of each target gene is relative to the amplification of the target gene in the WT strain, set to 1. Error bars represent the upper and lower range between experimental triplicates and averaged among biological duplicates.

| | AibA | AibB | LuxP | LsrB |
|---|---|---|---|---|
| **AibA** | 100.00 | 21.14 | 12.88 | 10.59 |
| **AibB** | 21.14 | 100.00 | 8.09 | 9.22 |
| **LuxP** | 12.88 | 8.09 | 100.00 | 9.97 |
| **LsrB** | 10.59 | 9.22 | 9.97 | 100.00 |

**Figure A4: Percent identity matrix between known AI-2 binding proteins.** Percent identity matrix determined by ClusalW2 sequence alignment between *H. pylori* G27 AibA, AibB, *Vibrio cholerae* LuxP, and *E. coli* LsrB. Numbers indicate the level of similarity between pairs of proteins from 0 (no similarity) to 100 (identical).

*Methods*

**Measuring AI-2 production in *H. pylori*.** WT, *luxS*$^{OP}$, and Δ*luxS H. pylori* cultures were inoculated into 3 ml BB10 from plate. Four hours after inoculation, cultures were diluted

back to $5x10^7$ cells $ml^{-1}$ and incubated shaking at 37°C, 10% $CO_2$. Samples of WT and *luxS*$^{OP}$ were taken at 4, 8, 12, 24, 36, and 48 hours post dilution and analyzed for optical density and colony forming units on plate. Samples of WT, *luxS*$^{OP}$ and Δ*luxS* were taken at each time point, spun down at 13500 rpm for 3 minutes, and the cell free supernatant (CFS) was saved and stored at -20°C. The CFS was analyzed for AI-2 using the *Vibrio harveyi* luminescence assay. 10 µl of CFS was added to 90 µl of *V. harveyi* culture (prepared as previously described for AI-2 binding assay) with duplicate samples in a 96-well plate. Levels of luminescence were measured on a SpectraMax M5e plate reader (Molecular Devices) each hour over the course of 6 hours with incubation on a shaker at 30°C in between measurements. Relative luminescence units (RLUs) were taken at the time point where there was the largest difference between an exogenous DPD positive control and the Δ*luxS* negative control.

**cDNA synthesis.** WT, Δ*aibA, aibA*,* Δ*aibB, aibB*,* Δ*tlpB,* and *tlpB*$^{D114N}$ strains were inoculated into liquid BB10 media from plate and grown shaking to an $OD_{600}$ of 1. Cultures were spun at 4000 rpm to pellet cells, and resuspended in 700 µL TRIzol reagent (Life Technologies). RNA was extracted following the TRIzol sample preparation protocol provided by the manufacturer, and the RNA pellet was resuspended in RNase-free water. The RNA was treated with DNase-1 (New England BioLabs) to degrade contaminant genomic DNA following the manufacturer's protocol. 5 µg RNA, 50 ng/µl random hexamer primers and SuperScript III Reverse Transcriptase (Life Technologies) were used to generate cDNA following the manufacturer's protocol. The resulting cDNA was treated with RNase H (Life Technologies) to degrade template RNA.

**qRT-PCR**. Synthesized cDNA was amplified using primers targeting ~100 base pair sequences of *aibA, aibB,* and *tlpB* genes, with *ureA* and *ureB* targets as endogenous controls. Primer efficiency was confirmed to be > 95% for each primer set used. qRT-PCR reactions contained 5 µl KAPA SYBR FAST qPCR Master Mix (Kapa Biosystems), 1 µl cDNA, 10 µM forward and reverse primers, and water to 10 µl reaction volume. Standard qRT-PCR reactions were performed in experimental triplicates on an Applied Biosystems StepOnePlus PCR machine (Life Technologies) and analyzed using StepOne software (version 2.2.2) to calculate relative quantity of target cDNA in mutant and complement strains to WT using both *ureA* and *ureB* as endogenous controls.

**Protein sequence alignment.** Gene and protein sequence for *H. pylori* G27 AibA (HPG27_277 hbpA) and AibB (HPG27_431 modA) were acquired from the UCSC Microbial Genome Browser (91). Representative LuxP (*Vibrio cholerae*, GenBank KFE33015.1) and LsrB (*Escherichia coli 101-1*, GenBank EDX40441.1) sequences were aligned with AibA and AibB using the ClustalW2 multiple protein sequence alignment (EMBL-EBI).

REFERENCES CITED


1. Suerbaum S, Michetti P. 2002. Helicobacter pylori infection. N. Engl. J. Med. 347:1175–1186.

2. Suzuki R, Shiota S, Yamaoka Y. 2012. Molecular epidemiology, population genetics, and pathogenic role of Helicobacter pylori. Infect. Genet. Evol. 12:203–13.

3. Jones KR, Whitmire JM, Merrell DS. 2010. A tale of two toxins: Helicobacter pylori CagA and VacA modulate host pathways that impact disease. Front. Microbiol.

4. Amieva MR, El-Omar EM. 2008. Host-bacterial interactions in Helicobacter pylori infection. Gastroenterology 134:306–23.

5. Bray F, Ren JS, Masuyer E, Ferlay J. 2013. Global estimates of cancer prevalence for 27 sites in the adult population in 2008. Int. J. Cancer 132:1133–1145.

6. Release P. 2013. Latest world cancer statistics Global cancer burden rises to 14 . 1 million new cases in 2012 : Marked increase in breast cancers must be addressed. Int. Agency Res. Cancer, World Heal. Organ. 2012–2014.

7. Papastergiou V, Georgopoulos SD, Karatapanis S. 2014. Treatment of Helicobacter pylori infection: Meeting the challenge of antimicrobial resistance. World J. Gastroenterol. 20:9898–9911.

8. Stein M, Ruggiero P, Rappuoli R, Bagnoli F. 2013. Helicobacter pylori CagA: From Pathogenic Mechanisms to Its Use as an Anti-Cancer Vaccine. Front. Immunol. 4:328.

9. Blaser MJ, Perez-Perez GI, Kleanthous H, Cover TL, Peek RM, Chyou PH, Stemmermann GN, Nomura A. 1995. Infection with Helicobacter pylori strains possessing cagA is associated with an increased risk of developing adenocarcinoma of the stomach. Cancer Res. 55:2111–2115.

10. Arévalo-Galvis A, Trespalacios-Rangel AA, Otero W, Mercado-Reyes MM, Poutou-Piñales RA. 2012. Prevalence of cagA, vacA, babA2 and iceA genes in H. pylori strains isolated from Colombian patients with functional dyspepsia. Polish J. Microbiol. 61:33–40.

11. Palframan SL, Kwok T, Gabriel K. 2012. Vacuolating cytotoxin A (VacA), a key toxin for Helicobacter pylori pathogenesis. Front. Cell. Infect. Microbiol.

12. Faundez G, Troncoso M, Figueroa G. 2002. cagA and vacA in strains of Helicobacter pylori from ulcer and non-ulcerative dyspepsia patients. BMC Gastroenterol. 2:20.

13. Sheh A, Fox JG. 2013. The role of the gastrointestinal microbiome in Helicobacter pylori pathogenesis. Gut Microbes.

14. Chen G, Fournier RL, Varanasi S, Mahama-Relue PA. 1997. Helicobacter pylori survival in gastric mucosa by generation of a pH gradient. Biophys. J. 73:1081–1088.

15. Weeks DL, Eskandari S, Scott DR, Sachs G. 2000. A H+-Gated Urea Channel: The Link Between Helicobacter pylori Urease and Gastric Colonization. Sci. 287 :482–485.

16. Lertsethtakarn P, Ottemann KM, Hendrixson DR. 2011. Motility and chemotaxis in Campylobacter and Helicobacter. Annu. Rev. Microbiol. 65:389–410.

17. Kusters JG, Kusters JG, van Vliet AHM, van Vliet AHM, Kuipers EJ, Kuipers EJ. 2006. Pathogenesis of Helicobacter pylori infection. Clin. Microbiol. Rev. 19:449–90.

18. Tan S, Noto JM, Romero-Gallo J, Peek RM, Amieva MR. 2011. Helicobacter pylori perturbs iron trafficking in the epithelium to grow on the cell surface. PLoS Pathog. 7:e1002050.

19. Howitt MR, Lee JY, Lertsethtakarn P, Vogelmann R, Joubert L, Ottemann KM. 2011. ChePep Controls Helicobacter pylori Infection of the Gastric Glands and Chemotaxis in the Epsilonproteobacteria 2:1–10.

20. Rader BA, Wreden C, Hicks KG, Sweeney EG, Ottemann KM, Guillemin K. 2011. Helicobacter pylori perceives the quorum-sensing molecule AI-2 as a chemorepellent via the chemoreceptor TlpB. Microbiology 157:2445–55.

21. Schauder S, Shokat K, Surette MG, Bassler BL. 2001. The LuxS family of bacterial autoinducers: Biosynthesis of a novel quorum-sensing signal molecule. Mol. Microbiol. 41:463–476.

22. Rutherford ST, Bassler BL. 2012. Bacterial quorum sensing: its role in virulence and possibilities for its control. Cold Spring Harb. Perspect. Med. 2.

23. Wozniak DJ, Parsek MR. 2014. Surface-associated microbes continue to surprise us in their sophisticated strategies for assembling biofilm communities. F1000Prime Rep. 6:26.

24. De la Fuente-Núñez C, Reffuveille F, Fernández L, Hancock REW. 2013. Bacterial biofilm development as a multicellular adaptation: antibiotic resistance and new therapeutic strategies. Curr. Opin. Microbiol. 16:580–9.

25. Elias S, Banin E. 2012. Multi-species biofilms: living with friendly neighbors. FEMS Microbiol. Rev. 36:990–1004.

26. Donlan RM. 2002. Biofilms : Microbial Life on Surfaces. Emerg. Infect. Dis. 8:881–890.

27. Davey ME, O'Toole GA. 2000. Microbial Biofilms : from Ecology to Molecular Genetics. Microbiol. Mol. Biol. Rev. 64.

28. Kostakioti M, Hadjifrangiskou M, Hultgren SJ. 2013. Bacterial biofilms: development, dispersal, and therapeutic strategies in the dawn of the postantibiotic era. Cold Spring Harb. Perspect. Med. 3:a010306.

29. Flemming H-C, Wingender J. 2010. The biofilm matrix. Nat. Rev. Microbiol. 8:623–33.

30. Moreau-Marquis S, Stanton B, O'Toole G. 2008. Pseudomonas aeruginosa biofilm formation in the cystic fibrosis airway. Pulm Pharmacol Ther. 21:595–599.

31. Kaplan JB. 2010. Biofilm Dispersal : Mechanisms , Clinical Implications , and Potential Therapeutic Uses. Crit. Rev. Oral Biol. Med. 89:205–218.

32. Hall-Stoodley L, Stoodley P. 2005. Biofilm formation and dispersal and the transmission of human pathogens. Trends Microbiol. 13:7–10.

33. Li Y-H, Tian X. 2012. Quorum sensing and bacterial social interactions in biofilms. Sensors (Basel). 12:2519–38.

34. González JE, Keshavan ND. 2006. Messing with bacterial quorum sensing. Microbiol. Mol. Biol. Rev. 70:859–75.

35. Marketon M, Glenn S. 2003. Quorum sensing controls exopolysaccharide production in Sinorhizobium meliloti. J. Bacteriol. 185:325–331.

36. Parsek MR, Greenberg E. 1999. Quorum sensing signals in development of Pseudomonas aeruginosa biofilms. Methods Enzym. 310:43–55.

37. Spoering AL, Gilmore MS. 2006. Quorum sensing and DNA release in bacterial biofilms. Curr. Opin. Microbiol. 9:133–7.

38. Boles BR, Horswill AR. 2008. Agr-mediated dispersal of Staphylococcus aureus biofilms. PLoS Pathog. 4:e1000052.

39. Claessen D, Rozen DE, Kuipers OP, Søgaard-Andersen L, van Wezel GP. 2014. Bacterial solutions to multicellularity: a tale of biofilms, filaments and fruiting bodies. Nat. Rev. Microbiol. 12:115–24.

40. Monds RD, O'Toole GA. 2009. The developmental model of microbial biofilms: ten years of a paradigm up for review. Trends Microbiol. 17:73–87.

41. Kaiser D. 2003. Coupling cell movement to multicellular development in myxobacteria. Nat. Rev. Microbiol. 1:45–54.

42. Hegde M, Englert DL, Schrock S, Cohn WB, Vogt C, Wood TK, Manson MD, Jayaraman A. 2011. Chemotaxis to the quorum-sensing signal AI-2 requires the Tsr chemoreceptor and the periplasmic LsrB AI-2-binding protein. J. Bacteriol. 193:768–73.

43. Stark R, Gerwig G. 1999. Biofilm formation by Helicobacter pylori. Lett Appl Microbiol. 28:121–126.

44. Cole S, Harwood J, Lee R. 2004. Characterization of monospecies biofilm formation by Helicobacter pylori. J. Bacteriol. 186:3124–3132.

45. Carron MA, Tran VR, Sugawa C, Coticchia JM. 2006. Identification of Helicobacter pylori Biofilms in Human Gastric Mucosa. J. Gastrointest. Surg. 10:712–717.

46. Coticchia JM, Sugawa C, Tran VR, Gurrola J, Kowalski E, Carron MA. 2006. Presence and density of Helicobacter pylori biofilms in human gastric mucosa in patients with peptic ulcer disease. J. Gastrointest. Surg. 10:883–889.

47. García A, Salas-Jara MJ, Herrera C, González C. 2014. Biofilm and Helicobacter pylori: from environment to human host. World J. Gastroenterol. 20:5632–8.

48. Karperien A. FracLac for ImageJ.

49. Tolle CR, McJunkin TR, Rohrbaugh DT, LaViolette RA. 2003. Lacunarity definition for ramified data sets based on optimal cover. Phys. D Nonlinear Phenom. 179:129–152.

50. Vendeville A, Winzer K, Heurlier K, Tang CM, Hardie KR. 2005. Making "sense" of metabolism: autoinducer-2, LuxS and pathogenic bacteria. Nat. Rev. Microbiol. 3:383–396.

51. Altschul SF, Gish W, Miller W, Myers EW, Lipman DJ. 1990. Basic local alignment search tool. J. Mol. Biol. 215:403–410.

52. Szurmant H, Ordal GW. 2004. Diversity in Chemotaxis Mechanisms among the Bacteria and Archaea Diversity in Chemotaxis Mechanisms among the Bacteria and Archaea. Microbiol. Mol. Biol. Rev. 68.

53. Miller ST, Xavier KB, Campagna SR, Taga ME, Semmelhack MF, Bassler BL, Hughson FM. 2004. Salmonella typhimurium recognizes a chemically distinct form of the bacterial quorum-sensing signal AI-2. Mol. Cell 15:677–87.

54. Chen X, Schauder S, Potier N. 2002. Structural identification of a bacterial quorum-sensing signal containing boron. Nature 5:545–549.

55. Sweeney EG, Henderson JN, Goers J, Wreden C, Kevin G, Foster JK, Parthasarathy R, Remington SJ, Guillemin K. 2012. Structure and proposed mechanism for the pH-sensing Helicobacter pylori chemoreceptor TlpB. Cell Struct. 20:1177–1188.

56. Rader BA, Campagna SR, Semmelhack MF, Bassler BL, Guillemin K. 2007. The quorum-sensing molecule autoinducer 2 regulates motility and flagellar morphogenesis in Helicobacter pylori. J. Bacteriol. 189:6109–17.

57. Amieva MR, Vogelmann R, Covacci A, Tompkins LS, Nelson J, Falkow S. 2003. Disruption of the epithelial apical-junctional complex by Helicobacter pylori CagA. Science (80-. ). 300:1430–1434.

58. Neiditch MB, Federle MJ, Miller ST, Bassler BL, Hughson FM. 2005. Regulation of LuxPQ receptor activity by the quorum-sensing signal autoinducer-2. Mol. Cell 18:507–518.

59. Pereira CS, de Regt AK, Brito PH, Miller ST, Xavier KB. 2009. Identification of functional LsrB-like autoinducer-2 receptors. J. Bacteriol. 191:6975–87.

60. Brillet K, Ruffenach F, Adams H, Journet L, Gasser V, Hoegy F, Guillon L, Hannauer M, Page A, Schalk IJ. 2012. An ABC transporter with two periplasmic binding proteins involved in iron acquisition in Pseudomonas aeruginosa. ACS Chem. Biol. 7:2036–45.

61. McDougald D, Rice SA, Barraud N, Steinberg PD, Kjelleberg S. 2012. Should we stay or should we go: mechanisms and ecological consequences for biofilm dispersal. Nat. Rev. Microbiol. 10:39–50.

62. Nijland R, Hall MJ, Burgess JG. 2010. Dispersal of biofilms by secreted, matrix degrading, bacterial DNase. PLoS One 5:e15668.

63. Kaplan JB. 2009. Therapeutic potential of biofilm-dispersing enzymes. Int. J. Artif. Organs.

64. Williams SM, Chen Y-T, Andermann TM, Carter JE, McGee DJ, Ottemann KM. 2007. Helicobacter pylori chemotaxis modulates inflammation and bacterium-gastric epithelium interactions in infected mice. Infect. Immun. 75:3747–57.

65. Cellini L, Grande R, Traini T, Di Campli E, Di Bartolomeo S, Di Iorio D, Caputi S. 2005. Biofilm formation and modulation of luxS and rpoD expression by Helicobacter pylori. Biofilms 2:119–127.

66. Cellini L, Grande R, Di Campli E, Di Bartolomeo S, Di Giulio M, Traini T, Trubiani O. 2008. Characterization of an Helicobacter pylori environmental strain. J. Appl. Microbiol. 105:761–769.

67. Abee T, Kovács ÁT, Kuipers OP, van der Veen S. 2011. Biofilm formation and dispersal in Gram-positive bacteria. Curr. Opin. Biotechnol.

68. Niu C, Robbins CM, Pittman KJ, Osborn DL, Stubblefield BA, Simmons RB, Gilbert ES. 2013. LuxS influences Escherichia coli biofilm formation through autoinducer-2-dependent and autoinducer-2-independent modalities. FEMS Microbiol. Ecol. 83:778–91.

69. Ali SA, Benitez J a. 2009. Differential response of Vibrio cholerae planktonic and biofilm cells to autoinducer 2 deficiency. Microbiol. Immunol. 53:582–6.

70. Hsiao A, Ahmed MS, Subramanian S, Griffin NW, Drewry LL, Petri WA, Haque R, Ahmed T, Gordon JI. 2014. Members of the human gut microbiota involved in recovery from Vibrio cholerae infection. Nature.

71. Covacci A, Censini S. 1993. Molecular characterization of the 128-kDa immunodominant antigen of Helicobacter pylori associated with cytotoxicity and duodenal ulcer. Proc. Natl Acad Sci 90:5791–5795.

72. Smeets LC, Bijlsma JJ, Boomkens SY, Vandenbroucke-Grauls CM, Kusters JG. 2000. comH, a novel gene essential for natural transformation of Helicobacter pylori. J. Bacteriol. 182:3948–3954.

73. Chalker AF, Minehart HW, Hughes NJ, Koretke KK, Lonetto MA, Brinkman KK, Warren P V, Lupas A, Stanhope MJ, Brown JR, Hoffman PS. 2001. Systematic identification of selective essential genes in Helicobacter pylori by genome prioritization and allelic replacement mutagenesis. J. Bacteriol. 183:1259–68.

74. Rasband W. 2012. ImageJ. U. S. Natl. Institutes Heal. Bethesda, Maryland, USA //imagej.nih.gov/ij/.

75. Tamada M, Perez TD, Nelson WJ, Sheetz MP. 2007. Two distinct modes of myosin assembly and dynamics during epithelial wound closure. J. Cell Biol. 176:27–33.

76. Pentecost M, Otto G, Theriot J a, Amieva MR. 2006. Listeria monocytogenes invades the epithelial junctions at sites of cell extrusion. PLoS Pathog. 2:e3.

77. Team R. 2012. R: A language and environment for statistical computing.

78. Zhang Y. 2008. I-TASSER server for protein 3D structure prediction. BMC Bioinformatics 9:40.

79. Marchler-Bauer A, Lu S, Anderson JB, Chitsaz F, Derbyshire MK, DeWeese-Scott C, Fong JH, Geer LY, Geer RC, Gonzales NR, Gwadz M, Hurwitz DI, Jackson JD, Ke Z, Lanczycki CJ, Lu F, Marchler GH, Mullokandov M, Omelchenko M V., Robertson CL, Song JS, Thanki N, Yamashita RA, Zhang D, Zhang N, Zheng C, Bryant SH. 2011. CDD: A Conserved Domain Database for the functional annotation of proteins. Nucleic Acids Res. 39.

80. Tam R, Saier MH. 1993. Structural, functional, and evolutionary relationships among extracellular solute-binding receptors of bacteria. Microbiol. Rev. 57:320–346.

81. Munshi P, Stanley CB, Ghimire-Rijal S, Lu X, Myles D a, Cuneo MJ. 2013. Molecular details of ligand selectivity determinants in a promiscuous β-glucan periplasmic binding protein. BMC Struct. Biol. 13:18.

82. Berntsson RPA, Smits SHJ, Schmitt L, Slotboom DJ, Poolman B. 2010. A structural classification of substrate-binding proteins. FEBS Lett.

83. Moon H, Lim H. 2015. ScienceDirect Synthesis and screening of small-molecule a -helix mimetic libraries targeting protein – protein interactions. Curr. Opin. Chem. Biol. 24:38–47.

84. Porter SL, Wadhams GH, Armitage JP. 2011. Signal processing in complex chemotaxis pathways. Nat. Rev. Microbiol. 9:153–165.

85. Kossmann M, Wolff C, Manson MD. 1988. Maltose chemoreceptor of Escherichia coli: interaction of maltose-binding protein and the tar signal transducer. J. Bacteriol. 170:4516–4521.

86. Zhang Y, Gardina PJ, Kuebler AS, Kang HS, Christopher JA, Manson MD. 1999. Model of maltose-binding protein/chemoreceptor complex supports intrasubunit signaling mechanism. Proc. Natl. Acad. Sci. U. S. A. 96:939–944.

87. Manson MD, Boos W, Bassford PJ, Rasmussen BA. 1985. Dependence of maltose transport and chemotaxis on the amount of maltose-binding protein. J. Biol. Chem. 260:9727–9733.

88. Sourjik V, Vaknin A, Shimizu TS, Berg HC. 2007. In Vivo Measurement by FRET of Pathway Activity in Bacterial Chemotaxis. Methods Enzymol.

89. Baltrus DA, Guillemin K. 2006. Multiple phases of competence occur during the Helicobacter pylori growth cycle. FEMS Microbiol. Lett. 255:148–155.

90. Force A, Lynch M, Pickett FB, Amores A, Yan YL, Postlethwait J. 1999. Preservation of duplicate genes by complementary, degenerative mutations. Genetics 151:1531–1545.

91. Karolchik D. 2003. The UCSC Genome Browser Database. Nucleic Acids Res. 31:51–54.

92. Office of the Press Secretary. 2015. Office of the Vice President. FACT SHEET Pres. 2016 Budg. Propos. Hist. Invest. to Combat Antibiot. Bact. to Prot. Public Heal.

93. Chey WD, Wong BCY. 2007. American College of Gastroenterology guideline on the management of Helicobacter pylori infection. Am. J. Gastroenterol. 102:1808–1825.

94. Sasaki M, Ogasawara N, Utsumi K, Kawamura N, Kamiya T, Kataoka H, Tanida S, Mizoshita T, Kasugai K, Joh T. 2010. Changes in 12-Year First-Line Eradication Rate of Helicobacter pylori Based on Triple Therapy with Proton Pump Inhibitor, Amoxicillin and Clarithromycin. J. Clin. Biochem. Nutr. 47:53–58.

95. Bordi C, de Bentzmann S. 2011. Hacking into bacterial biofilms: a new therapeutic challenge. Ann Intensive Care 1:19.

96. Tang K, Zhang XH. 2014. Quorum quenching agents: Resources for antivirulence therapy. Mar. Drugs.

97. Chen G, Swem LR, Swem DL, Stauff DL, Loughlin CT, Jeffrey PD, Bassler BL, Hughson FM. 2011. A Strategy for Antagonizing Quorum Sensing. Mol. Cell 42:199–209.

98. Xavier KB, Bassler BL. 2005. Interference with AI-2-mediated bacterial cell-cell communication. Nature 437:750–753.

99. Packiavathy IASV, Priya S, Pandian SK, Ravi AV. 2014. Inhibition of biofilm development of uropathogens by curcumin - An anti-quorum sensing agent from Curcuma longa. Food Chem. 148:453–460.

100. O'Loughlin CT, Miller LC, Siryaporn A, Drescher K, Semmelhack MF, Bassler BL. 2013. A quorum-sensing inhibitor blocks Pseudomonas aeruginosa virulence and biofilm formation. Proc. Natl. Acad. Sci. U. S. A. 110:17981–6.

101. Blaser MJ. 2008. Disappearing Microbiota : Helicobacter pylori Protection against Esophageal Adenocarcinoma Disappearing Microbiota : Helicobacter pylori Protection against Esophageal Adenocarcinoma. Cancer Prev. Res. (Phila). 1:308–311.

102. Arnold IC, Hitzler I, Müller A. 2012. The Immunomodulatory Properties of Helicobacter pylori Confer Protection Against Allergic and Chronic Inflammatory Disorders. Front. Cell. Infect. Microbiol.